Biomaterials Science

ROYAL SOCIETY OF CHEMISTRY

PAPER

View Article Online
View Journal | View Issue

Check for updates

Cite this: *Biomater. Sci.*, 2024, **12**, 1822

Free drug and ROS-responsive nanoparticle delivery of synergistic doxorubicin and olaparib combinations to triple negative breast cancer models†

Robert J. Cavanagh,*[a] Patrícia F. Monteiro,[a,d] Cara Moloney,[a,b] Alessandra Travanut,[a] Fatemeh Mehradnia,[a] Vincenzo Taresco,[c] Ruman Rahman,[b] Stewart G. Martin,[b] Anna M. Grabowska,[b] Marianne B. Ashford[d] and Cameron Alexander*[a]

Combinations of the topoisomerase II inhibitor doxorubicin and the poly (ADP-ribose) polymerase inhibitor olaparib offer potential drug–drug synergy for the treatment of triple negative breast cancers (TNBC). In this study we performed *in vitro* screening of combinations of these drugs, administered directly or encapsulated within polymer nanoparticles, in both 2D and in 3D spheroid models of breast cancer. A variety of assays were used to evaluate drug potency, and calculations of combination index (CI) values indicated that synergistic effects of drug combinations occurred in a molar-ratio dependent manner. It is suggested that the mechanisms of synergy were related to enhancement of DNA damage as shown by the level of double-strand DNA breaks, and mechanisms of antagonism associated with mitochondrial mediated cell survival, as indicated by reactive oxygen species (ROS) generation. Enhanced drug delivery and potency was observed with nanoparticle formulations, with a greater extent of doxorubicin localised to cell nuclei as evidenced by microscopy, and higher cytotoxicity at the same time points compared to free drugs. Together, the work presented identifies specific combinations of doxorubicin and olaparib which were most effective in a panel of TNBC cell lines, explores the mechanisms by which these combined agents might act, and shows that formulation of these drug combinations into polymeric nanoparticles at specific ratios conserves synergistic action and enhanced potency *in vitro* compared to the free drugs.

Received 27th November 2023,
Accepted 14th February 2024

DOI: 10.1039/d3bm01931d

rsc.li/biomaterials-science

Open Access Article. Published on 15 Nyenyenyani 2024. Downloaded on 2024-09-11 19:17:30.
This article is licensed under a Creative Commons Attribution 3.0 Unported Licence.

Introduction

Breast cancer is a continuing global health concern, and despite advances in surgery and radiotherapy, there are still requirements for treatment when these options fail.[1] Triple negative breast cancer (TNBC) is a subtype of this disease, in which the expression of estrogen (ER) and progesterone receptors (PR) is reduced, and accounts for 15–20% of all breast cancer cases.[2,3] In addition, the human epidermal growth factor receptor 2 (HER 2) is not overexpressed as in other breast cancers, making TNBC particularly difficult to treat,[4–6] with poor prognoses and low overall survival.[7] The 5 years survival of TNBC patients is approximately 70%, compared to 90% in other breast cancer subtypes, and decreases to approximately 10% following disease metastasis.[8,9] Chemotherapy is long-established for use in treating breast cancers, but many current drugs have undesirable side-effects, including systemic toxicity and limited efficacy, particularly in TNBC. The therapeutic window of some of these drugs can be improved by the use of delivery vehicles, and liposomal formulations of the topoisomerase II inhibitor, doxorubicin, have been used in patients for over 25 years with clear benefits in terms of quality of life.[10]

Despite these successes, the heterogeneity of many cancers means that single agent chemotherapy is not always effective, and combination therapies are increasingly being used.[11] The combination of doxorubicin with the poly (ADP-ribose) polymerase (PARP) inhibitor, olaparib, has shown promising results in preclinical and early stage clinical studies, and

[a]*School of Pharmacy, University of Nottingham, NG7 2RD, UK.*
E-mail: robert.cavanagh1@nottingham.ac.uk, cameron.alexander@nottingham.ac.uk
[b]*School of Medicine, BioDiscovery Institute, University of Nottingham, NG7 2RD, UK*
[c]*School of Chemistry, University of Nottingham, NG7 2RD, UK*
[d]*Advanced Drug Delivery, Pharmaceutical Sciences, R&D, AstraZeneca, Macclesfield, UK*

† Electronic supplementary information (ESI) available. See DOI: https://doi.org/10.1039/d3bm01931d

This journal is © The Royal Society of Chemistry 2024

Open Access Article. Published on 15 Nyenyenyani 2024. Downloaded on 2024-09-11 19:17:30.
This article is licensed under a Creative Commons Attribution 3.0 Unported Licence.

recently olaparib has been evaluated in platinum-resistant ovarian cancer in combination with liposomal doxorubicin.[12] However, the differing pharmacokinetics of a small molecule free drug, compared to a liposomal carrier, introduces inherent complications in terms of dosing. In addition, the differences in cell entry mechanisms for drugs and nanoparticles[13] mean that overexpressed efflux pumps in certain cancer cell types might alter the relative intracellular concentrations of the drugs.[14]

As a consequence, there are some important potential advantages of encapsulating or conjugating combinations of drug molecules in a single carrier. The concept of co-delivery of drugs by polymer carriers and liposomes has been well-established *in vitro*[15,16] and recently has been extended to efficacy in humans.[17] Furthermore, the variety of mechanisms by which some anti-cancer drugs act mean that there can be advantages of co-delivery beyond avoidance of efflux pumps in resistant cell lines.[18] These can include directing drugs to specific intracellular targets to induce apoptotic pathways or sensitisation of the cell to other cytotoxic processes such as radiation.[19–22] There is accordingly a clear rationale for incorporating combinations of drugs in carriers for many cancers, and for breast cancer the specific combination of doxorubicin and olaparib, in the same nanoparticle. In previous studies it has been shown that TNBC cells can exhibit altered redox environments, with upregulation of intracellular glutathione.[23–25] However, it is also the case that reactive oxygen species (ROS) can be present in higher concentrations in TNBC compared to other breast cancer subtypes[26] and is believed to play a pro-tumorigenic role by maintaining the oncogenic signalling required for proliferation and survival.[27,28] Moreover, increased ROS generation may be induced therapeutically following radiotherapy, or *via* the action of chemotherapy drugs.[29,30] Polymer therapeutic and nanoparticle delivery systems have been designed to exploit abnormal redox environments in cancer cells by both reduction-sensitive[31–34] and oxidation-sensitive chemistries.[35,36] In this work we have evaluated combinations of doxorubicin and olaparib, delivered *via* nanoparticle carriers containing an oxidatively-cleavable thioketal group cross-linking the micellar-like cores, and demonstrate that the formulations retain the advantages of specific drug : drug ratios in synergistic cytotoxicity in TNBC cell lines.

Results

We set out initially to assess any synergistic or antagonistic effects of combinations of doxorubicin and olaparib, and then to encapsulate them in nanoparticulate carriers at ratios shown to be most active against a series of TNBC cell lines.

Effects of individual drugs on breast cancer cells

The potencies of doxorubicin (DOX) and olaparib (OLA) were studied in three breast cancer cells (BCC) lines, the luminal subtype line MCF-7 and the triple negative MDA-MB-231 and MDA-MB-468 breast cancer lines. Cells were cultured in standard 2D models and as 3D spheroid models. Measured drug potencies (Table 1) showed that in both 2D and spheroid culture models TNBC lines were relatively less sensitive to DOX than the luminal breast cancer line (MCF-7), with higher DOX IC_{50} values calculated in the latter. In general, OLA was determined to be approximately two orders of magnitude less cytotoxic than the DNA damaging agent DOX in the BCC lines tested. Comparison of IC_{50} values between cell cultures models, revealed that 3D spheroids were more resistant to DOX and OLA treatment than their 2D cultured counterparts, in accordance with prior literature;[37] DOX demonstrated approximately 6-fold, 18-fold and 29-fold increased resistance in MDA-MB-231, MDA-MB-468 and MCF-7 cells respectively, and OLA 2-fold, 8-fold and 5-fold increased resistance in MDA-MB-231, MDA-MB-468 and MCF-7 cells respectively, when comparing 2D to 3D spheroid culture.

Identification of synergistic DOX and OLA combinations

Following the assessment of single drug potency, the effects of DOX and OLA combinations were evaluated in the three cell lines over a 48-hour period. Drug combinations were investigated at 5 different molar ratios, and the combination index (CI) values were calculated for each ratio. In accordance with the median-effect algorithm established by Chou and Talalay,[38,39] CI values categorise and quantify drug–drug combinations at specific ratios as antagonistic (CI > 1.1), additive (CI = 0.9–1.1) or synergistic (CI < 0.9).

The CI results are presented in Fig. 1 as a heat map for each DOX : OLA ratio and demonstrate that drug–drug synergy occurred in a molar-ratio dependent manner. In the TNBC lines (MDA-MB-231 and MDA-MB-468), synergistic efficacy was observed at molar ratios wherein DOX was the dominant drug (100 : 1 and 10 : 1) or when applied at equal amounts with OLA (1 : 1). The highest synergy, as quantified by CI value, was observed in MDA-MB-231 cells at these ratios. Interestingly, only an additive effect was elicited at these molar ratios in the luminal MCF-7 cell line. At higher OLA ratios, antagonist effects were induced, or, in the case of MDA-MB-468 at 1 : 10 (DOX : OLA), additive effects. It can be noted that stronger antagonistic effects, as denoted by increasing CI values, were induced at the highest OLA ratio 1 : 100.

Table 1 Calculated drug IC_{50} values in 2D and 3D spheroid breast cancer cells. Drugs exposed to cells for 48 hours. Potency assessed *via* (2D) Prestoblue metabolic activity and (3D) spheroid ATP levels measured using CellTiter Glo 3D assay. IC_{50} values calculated *via* GraphPad Prism and dose response curves shown in ESI Fig. 1.† IC_{50} values presented as mean ± S.D

	2D cultured cells		3D cultured cells	
Cell line	Doxorubicin	Olaparib	Doxorubicin	Olaparib
MDA-MB-231	0.97 ± 0.15 μM	101 ± 13 μM	5.5 ± 1.0 μM	217 ± 28 μM
MDA-MB-468	0.23 ± 0.14 μM	28 ± 5.0 μM	4.1 ± 0.7 μM	213 ± 18 μm
MCF-7	0.09 ± 0.01 μM	74 ± 2.1 μM	2.6 ± 0.8 μM	343 ± 46 μM

Open Access Article. Published on 15 Nyenyenyani 2024. Downloaded on 2024-09-11 19:17:30.
This article is licensed under a Creative Commons Attribution 3.0 Unported Licence.

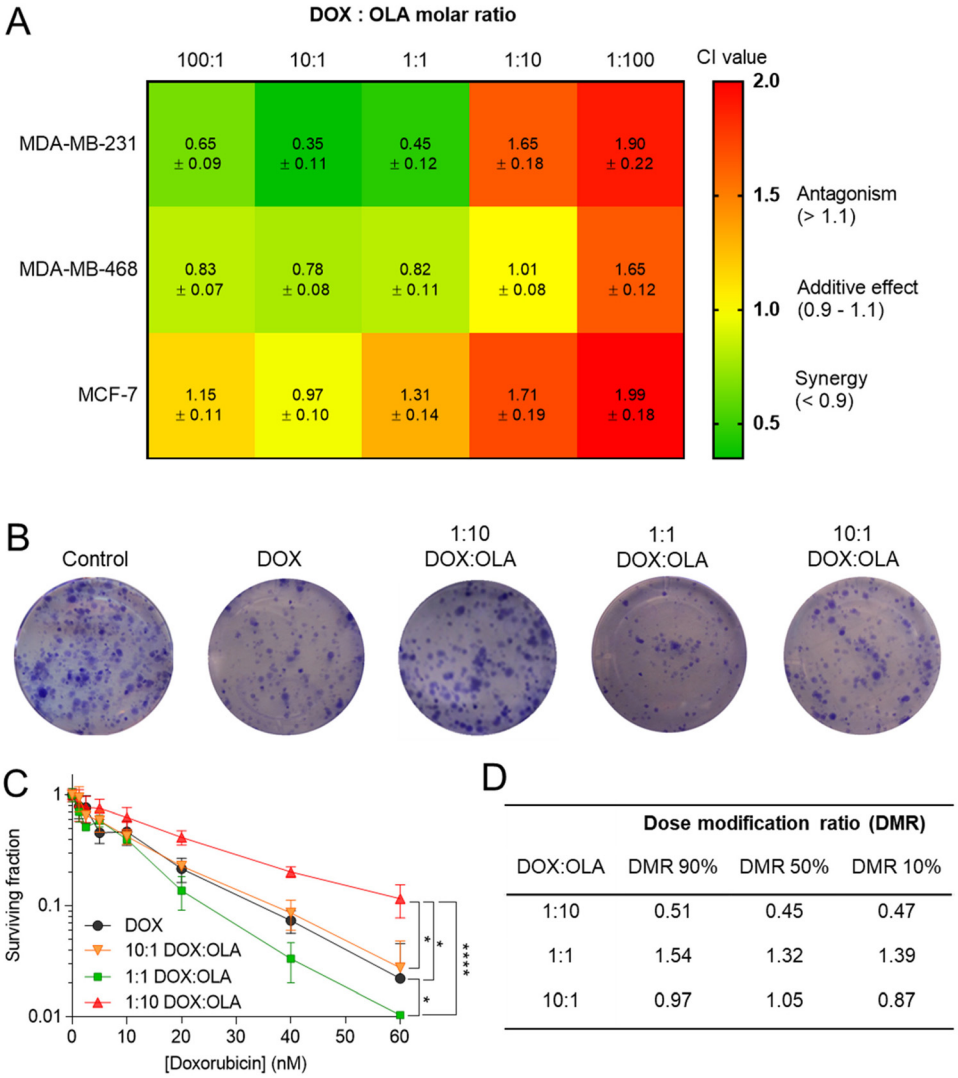

Fig. 1 (A) Combination index (CI) values (mean ± S.D) for DOX and OLA at different molar ratios using Tou and Chalay method for quantification of synergy.[38,39] Data generated from PrestoBlue metabolic assays following drug combination treatment. (B) Clonogenic survival assay in MDA-MB-231 cells, (C) subsequent dose–response plotting and (D) table of calculated dose modification ratio. Statistical significance tested using two-way ANOVA and Tukey's multiple comparisons tests (*, $p < 0.05$; ****, $p < 0.0001$).

These initial observations were made using a metabolic activity-based assay (PrestoBlue™), and thus to derive further mechanistic detail, clonogenic survival assays were undertaken in MDA-MB-231 cells, whereby the capability of a single cell to form a colony was assessed following single or combination drug therapy. Levels of cytotoxicity in cells treated with DOX were approximately three orders of magnitude greater than in cells treated with OLA, with significant inhibition of colony formation observed at concentrations ≥5.0 nM and ≥2.5 μM for DOX and OLA, respectively (Fig. 1 and ESI Fig. 2†). Molar ratios 10 : 1, 1 : 1 and 1 : 10 (DOX : OLA) at DOX concentrations in a range of 0.6–60 nM were then applied and the effects on colony formation measured. Significantly decreased colony survival was observed at molar ratios of 1 : 1 and significantly increased survival noted at 1 : 10 when compared to DOX alone treatment. Dose modification ratios (DMR) of DOX : OLA combinations compared to DOX alone indicate an antagonistic effect with 1 : 10 combination (DMR < 1), synergistic effects with 1 : 1 (DMR > 1), and additive effects with 10 : 1 (DMR ≈ 1).

In order to study DOX : OLA combinations in a more physiologically relevant model, 3D spheroids of MCF-7, MDA-MB-231 and MDA-MB-468 were generated. Displayed in Fig. 2 as a heat map, the CI values of DOX : OLA combinations indicated similar trends to those observed in 2D cultured cells. Namely, in MDA-MB-231 and MDA-MB-468 TNBC spheroids, synergy was observed in molar ratios higher in DOX (100 : 1 and 10 : 1) or equal drug ratios (1 : 1), and antagonism induced at higher OLA ratios (1 : 10 and 1 : 100). Again, as with 2D models, MCF-7 spheroids only demonstrated additive effects (at 100 : 1, 10 : 1 and 1 : 1) or antagonistic effects (1 : 10 and 1 : 100). These

 This journal is © The Royal Society of Chemistry 2024

Open Access Article. Published on 15 Nyenyenyani 2024. Downloaded on 2024-09-11 19:17:30.
This article is licensed under a Creative Commons Attribution 3.0 Unported Licence.

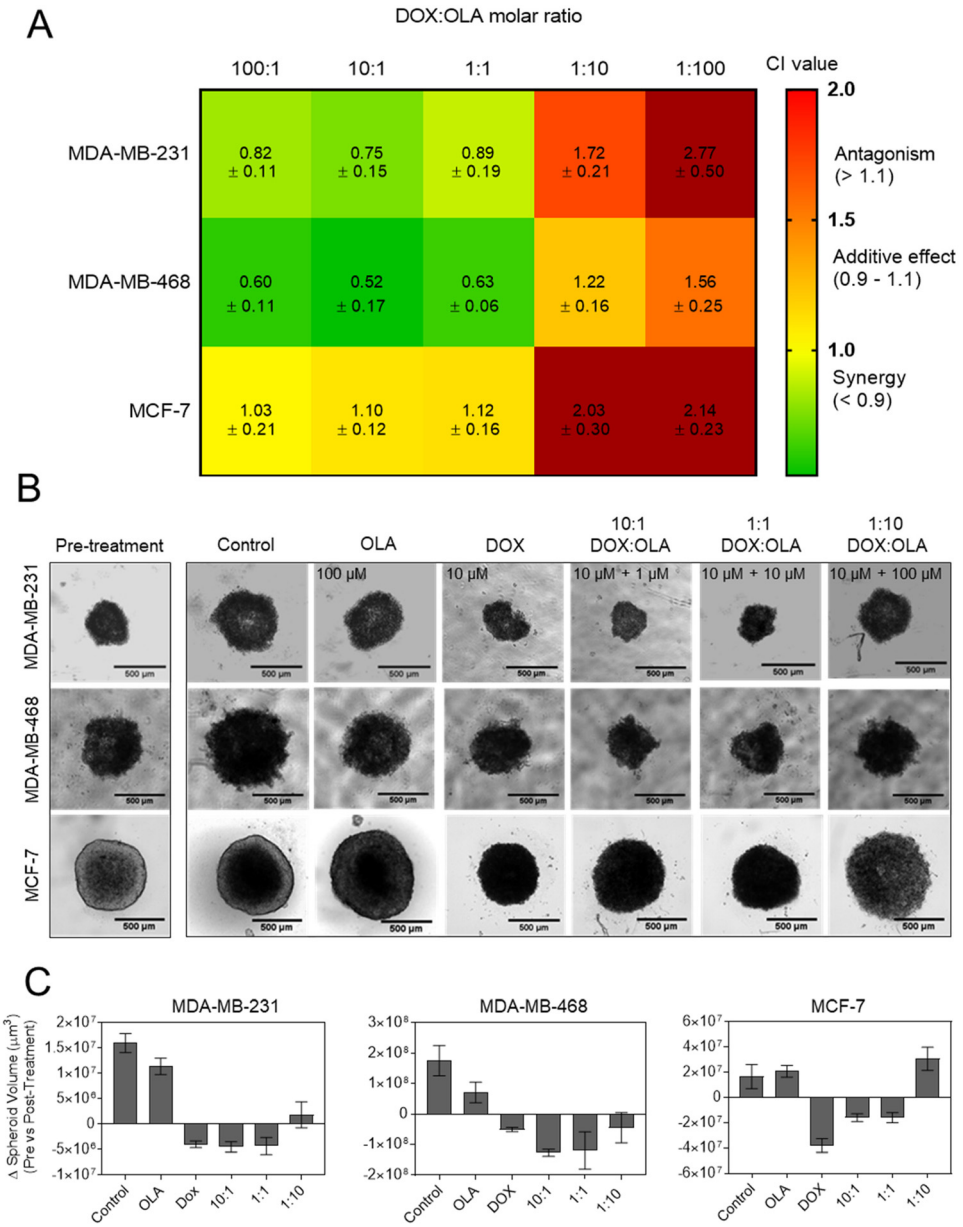

Fig. 2 Synergism of DOX : OLA combinations in 3D BCCs spheroid models. (A) CI values generated following treatment and assaying with CellTiter Glo 3D probing cellular ATP levels. (B) Micrographs of spheroid morphologies pre- and post-treatment (72 h exposure) and (C) subsequent spheroid volume analysis. Scale bar is 500 µm and volume change presented as mean ± S.D.

observations made in spheroids *via* ATP level measurement (CellTiter Glo 3D assay), and subsequent IC_{50} and CI value calculations, were supported by morphological and spheroid volume analysis performed *via* microscopy (Fig. 2).

Apoptosis assessment with caspase activation

Following measurements of drug potency *via* metabolic activities and cell survival, the potential of DOX, OLA and DOX : OLA combinations to induce apoptosis was studied in MDA-MB-231 cells *via* the measurement of caspase-3/7 activation (Fig. 3). DOX applied at a concentration of 10 nM induced significant caspase-3/7 activation, relative to untreated control. OLA was shown to require concentrations ≥10 µM to induce significant caspase-3/7 activation (ESI Fig. 3†). When solutions of 10 nM DOX were supplemented with either 1 or 10 nM OLA, to represent combination molar ratios of 10 : 1 and 1 : 1 (DOX : OLA) respectively, enhanced caspase activation was observed relative to the single drug controls (Fig. 3A and B). However, application of 10 nM DOX in combination with 100 nM OLA (representing 1 : 10 DOX : OLA ratio) resulted in the abolishment of caspase activation, reducing levels to those comparable to the vehicle control (Fig. 3C). Indeed, the 1 : 10 (DOX : OLA) combination was observed to required drug concentrations 100-fold higher (1 µM DOX + 10 µM OLA) in order

Open Access Article. Published on 15 Nyenyenyani 2024. Downloaded on 2024-09-11 19:17:30.
This article is licensed under a Creative Commons Attribution 3.0 Unported Licence.

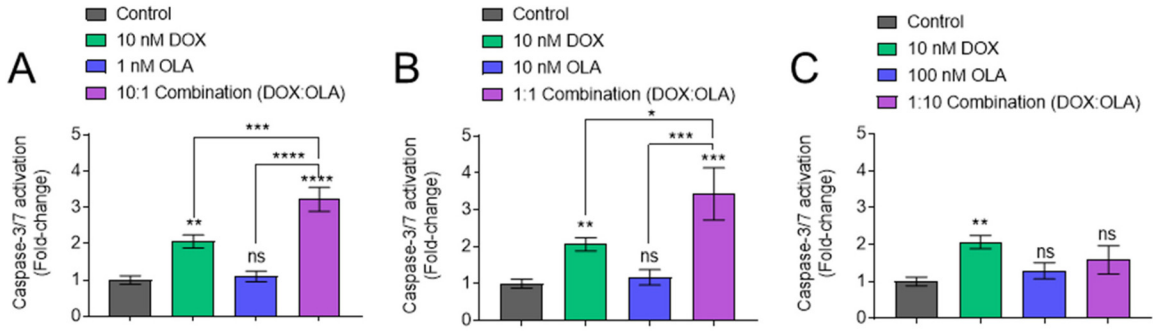

Fig. 3 Detection of caspase-3/7 activation. MDA-MB-231 cells cultured in 2D manner and incubated with single, combination or the vehicle control for 24 hours. Levels of caspase-3/7 activation were then probed using CellEvent caspase-3/7 detection reagent. Variations in dosing of OLA compared to DOX are shown in (A), 1 nm OLA;, (B) 10 nM OLA, and (C) 100 nm OLA. Values normalised to vehicle control. Statistical significance tested using one-way ANOVA and Dunnett's multiple comparisons tests (*, $p < 0.05$; **, $p < 0.005$; ***, $p < 0.0005$; ****, $p < 0.0001$). Data presented as mean ± S.D.

to induce levels of caspase activation that were significantly higher than single DOX treatment (ESI Fig. 3†). Together, the caspase-3/7 activation assays supported the noted molar ratio-dependency of synergy or antagonism with DOX : OLA combinations observed in 2D and 3D cytotoxicity experiments (Fig. 1 and 2).

Investigation of mechanisms for synergistic drug combination efficacy

To investigate the mechanism of synergy of the DOX and OLA combinations, the level of double stranded DNA breaks (DSBs) was assessed in MDA-MB-231 and MCF-7 cells using the γH2AX assay (Fig. 4). The data demonstrated that 1 μM DOX induced significantly increased levels of γH2AX foci, indicating increased DSBs, compared to the untreated controls for both cell lines. Treatment with OLA generated significant increases in γH2AX foci at concentrations of 1 and 10 μM but not for 0.1 μM OLA in both MDA-MB-231 and MCF-7 cells. In MCF-7 cells, DOX and OLA combinations, tested at molar ratios of 10 : 1, 1 : 1 and 1 : 10, did not elicit any significant increases in γH2AX foci relative to DOX mono-treatment (Fig. 4). Indeed, only comparable γH2AX foci numbers were seen at 10 : 1 (foci, 38 ± 8) and 1 : 1 DOX : OLA (foci, 39 ± 13) combinations compared to DOX (foci, 43 ± 15), and a non-significant ($P = 0.31$), decrease in foci at the 1 : 10 combination (foci, 32 ± 5). Together with previously calculated CI values (Fig. 1 and 2), the γH2AX assay thus indicated that only additive or antagonist effects were induced by DOX and OLA combinations in MCF-7 luminal breast cancer cells. In MDA-MB-231 cells, significant increases in γH2AX foci were observed with DOX and OLA combinations compared to treatment with DOX alone (foci, 43 ± 7). Notably, a significant increase with 10 : 1 (foci, 63 ± 11; $P = 0.055$) and 1 : 1 (foci, 89 ± 11; $P = 0.004$) DOX : OLA combinations, combinations that were previously determined synergistic *via* CI calculations (Fig. 1 and 2). The 1 : 10 DOX : OLA combination, in support with antagonistic CI values, induced significantly decreased γH2AX foci (foci, 23 ± 3; $P = 0.011$) relative to the DOX mono-treatment control.

Investigation of redox species induction *via* combination drug treatments

To explore the potential mitochondrial or redox mechanisms of DOX and OLA combinations, drug induced ROS generation was studied in MDA-MB-231 TNBC cells (Fig. 5). DOX has been previously found to increase intracellular ROS generation *via* redox cycling and the Fenton reaction.[40] In MDA-MB-231 cells it can be observed that significant increases in ROS, as determined by the CM-H2DCFA assay, were induced, in an approximately linear time-dependent manner, within the first 60 minutes of exposure to 1 μM DOX (Fig. 5A). On the other hand, OLA was observed to induce a transient ROS spike evident at 15 minutes of exposure which subsided to basal levels by 30 minutes. The ROS spike appeared to be concentration dependent, with the largest magnitude observed to approx. 2-Fold basal levels with 10 μM OLA, 1.5-fold with 1 μM OLA, and a slight, but significant increase to 1.2-fold with 0.1 μM OLA (Fig. 5A). Following the OLA-induced ROS burst at 15 minutes, no further significant increase in ROS was observed with OLA within a 60-minute time frame. For drug combination treatments, intracellular ROS profiles demonstrated aspects of both DOX and OLA in an exposure time-dependent manner. Notably, for 1 μM DOX with 1 μM OLA or 10 μM OLA (1 : 1 and 1 : 10 molar ratios, respectively), the transient ROS burst at 15 minutes was experienced in a comparable manner to OLA alone treatment. ROS levels subsequently returned to basal levels at 30 minutes, as observed with OLA treatment, followed by an increase in ROS levels observed at 60 minutes. This latter ROS increase was likely resulting from the effects of DOX, which in DOX-only treatments increased ROS at this time point. In DOX : OLA combinations, this DOX-associated ROS generation at 60 minutes appeared significantly lower in DOX combinations with 1 μM OLA or 10 μM OLA than in DOX alone treatment. Together, the data thus indicated that OLA might suppress DOX-mediated ROS generation when applied at these concentrations.

To investigate further, mitochondrial membrane potentials ($\Delta\Psi_m$) were studied using a JC-1 assay (Fig. 5B and C). When

This journal is © The Royal Society of Chemistry 2024

Open Access Article. Published on 15 Nyenyenyani 2024. Downloaded on 2024-09-11 19:17:30.
This article is licensed under a Creative Commons Attribution 3.0 Unported Licence.

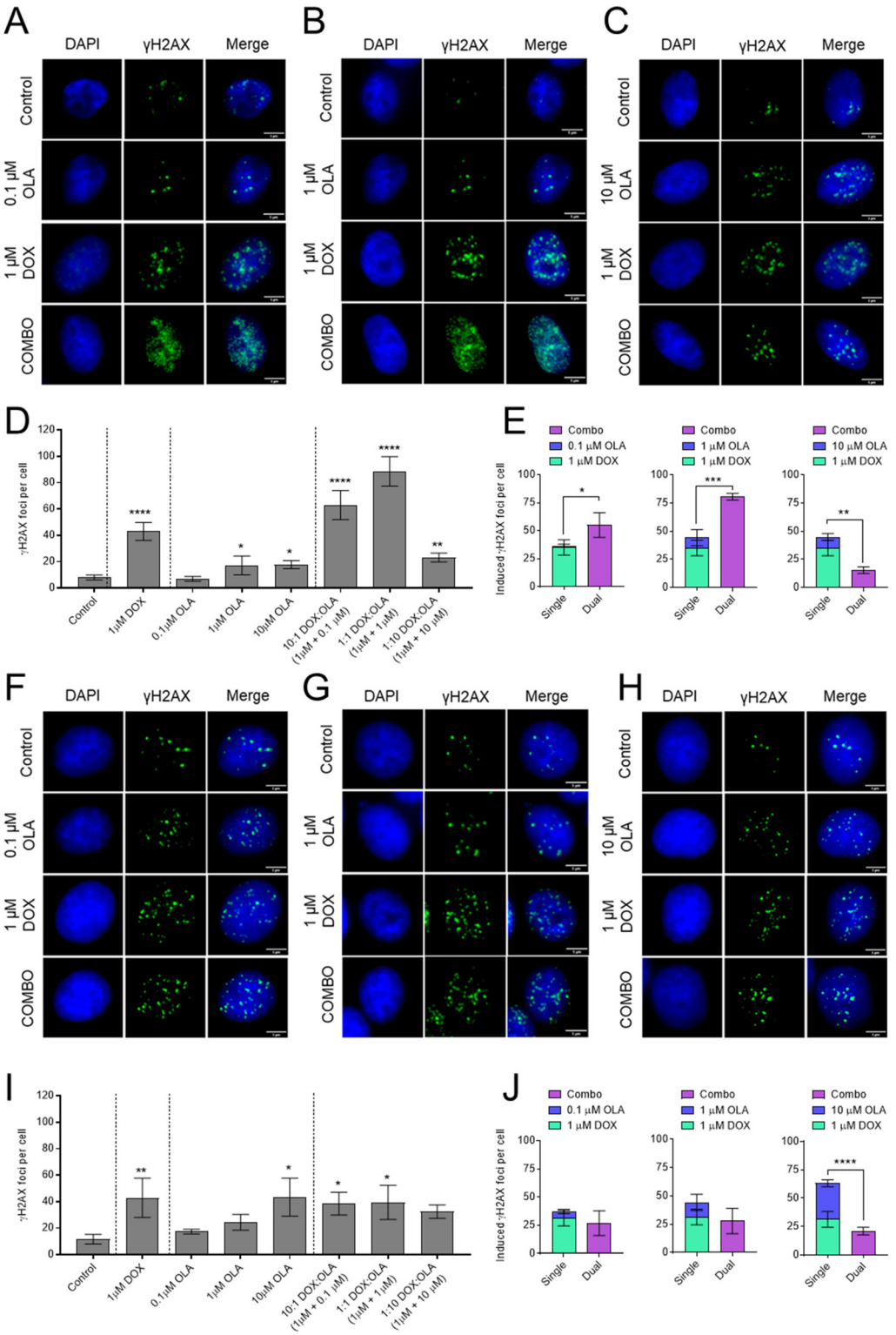

Fig. 4 Immunofluorescence microscopy of γH2AX foci as a marker of dsDNA breaks in (A–E) MDA-MB-231 and (F–J) MCF-7cells. Cells exposed to single dosed DOX (1 μM), OLA (0.1–10 μM) and DOX : OLA combinations for 24 hours. DOX concentration was kept constant at 1 μM and OLA concentration ranged from (A and F) 0.1 μM, (B and G) 1 μM, and (C and H) 10 μM as either single drug or in combination with DOX, to represent DOX : OLA combinations of 10 : 1, 1 : 1 and 1 : 10, respectively. Scale bar, 5 μm. (D and I) Foci quantification was performed using ImageJ and data presented in bar charts (mean ± S.D). (E and J) Induced foci per cell data presented for response additivity analysis. Statistical significance tested using one-way ANOVA and Dunnett's multiple comparisons tests to compare (D and I) treatments to control and, (E and J) summation of single treatments to combination treatments (*, $p < 0.05$; **, $p < 0.005$; ***, $p < 0.0005$; ****, $p < 0.0001$).

Open Access Article. Published on 15 Nyenyenyani 2024. Downloaded on 2024-09-11 19:17:30.
This article is licensed under a Creative Commons Attribution 3.0 Unported Licence.

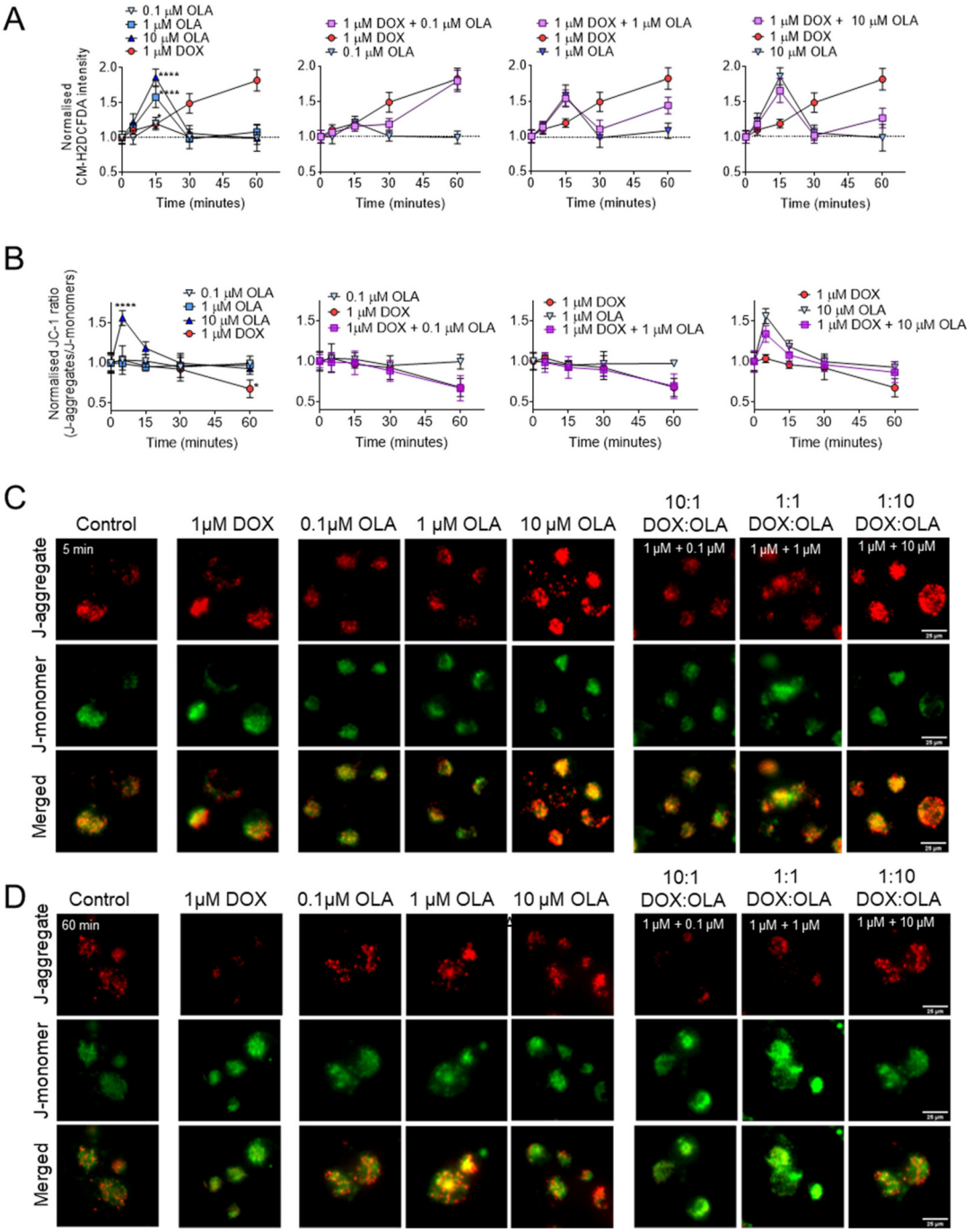

Fig. 5 Mitochondrial effects of single drugs and drug combinations in MDA-MB-231 cells. (A) Intracellular ROS generation assessed with CM-H2DCFA. (B) Mitochondrial membrane potential measured using JC-1 assay and accompanying JC-1 images captured at (C) 5 minutes and (D) 60 minutes of exposure. Data presented as mean ± S.D. Scale bar is 25 μm.

applied as mono-treatment, 1 μM DOX was observed to induce significant $\Delta\Psi_m$ depolarisation at 60 minutes of drug exposure. In addition to DOX-mediated DNA damage, overproduction of ROS is known to have detrimental effects on mitochondrial processes such as the electron transport chain and mitochondrial membrane permeability.[40] Thus, the DOX-mediated $\Delta\Psi_m$ depolarisation was likely a consequence of the observed DOX-associated ROS generation (Fig. 5A). Application of 0.1 μM and 1 μM OLA was not observed to induce any alterations in $\Delta\Psi_m$. However, 10 μM OLA was noted to elicit $\Delta\Psi_m$ hyperpolarisation in a transient manner, peaking at 5 minutes, with a decreased but still significant hyperpolarisation at 10 minutes and a return to baseline levels at 15 minutes of exposure. Interestingly, mitochondrial hyperpolarisation has been reported before with PARP inhibition and associated with conferring mitochondrial protection and cell

 This journal is © The Royal Society of Chemistry 2024

Open Access Article. Published on 15 Nyenyenyani 2024. Downloaded on 2024-09-11 19:17:30.
This article is licensed under a Creative Commons Attribution 3.0 Unported Licence.

survival.[41] In the current work, $\Delta\Psi_m$ hyperpolarisation appeared to precede the OLA-mediated ROS burst, suggesting both events may be associated, with $\Delta\Psi_m$ hyperpolarisation potentially driving increased mitochondrial ROS generation, an event that has been reported elsewhere, albeit under different conditions.[42]

In combinations of DOX and OLA, no significant differences were observed from the DOX alone treatment. A gradual $\Delta\Psi_m$ depolarisation was found when either 0.1 μM or 1 μM OLA were applied alongside 1 μM DOX (Fig. 5B). However, application of 10 μM OLA with 1 μM DOX, resulted in $\Delta\Psi_m$ hyperpolarisation at 5 minutes. This effect was similar, albeit reduced, relative to treatment with OLA alone, and was followed by an apparent $\Delta\Psi_m$ depolarisation at 60 minutes. This suggested that 10 μM OLA may have conferred some protection against the $\Delta\Psi_m$ depolarisation mediated by DOX at 60 minutes, an effect likely mediated by the reduced ROS generation noted with this combination at 60 minutes. Taken together, these data suggested that antagonism, observed in combinations where DOX < OLA (*i.e.* 1 : 10, 1 : 100), may have resulted from OLA-mediated mitochondrial protection. This phenomenon we associate with $\Delta\Psi_m$ hyperpolarisation, a consequent ROS spike, and ultimately a suppression of DOX-mediated ROS generation.

Nanoparticle formulation and uptake in BCCs

It has been suggested that some combination therapies may be enhanced by co-delivery of the therapeutic agents by a single carrier, so that variations in the individual pharmacokinetic profiles of the drugs can be avoided and simultaneous intracellular dosing achieved by the delivery agent. Thus, to investigate any synergies of drug combinations delivered intracellularly, we chose to prepare polymeric nanoparticles as delivery vehicles for the drug combinations. For the architectures and chemistries of the carriers, we selected micellar-like nanoparticles, employing a poly(ethyleneglycol) component to provide colloidal stability and reduce protein adsorption, and a mixed poly(D,L-lactide-*co*-2-azidocaprolactone) block with the pendant azide groups installed (Fig. 6) to enable facile core-cross-linking *via* click chemistries.[43] The synthetic strategy was adapted from that which we used for reduction-responsive polymers for docetaxel delivery in TNBC,[44] but in this case we prepared an oxidatively-sensitive dithioketal[45] between the cross-link points to replace the disulfide linker we employed

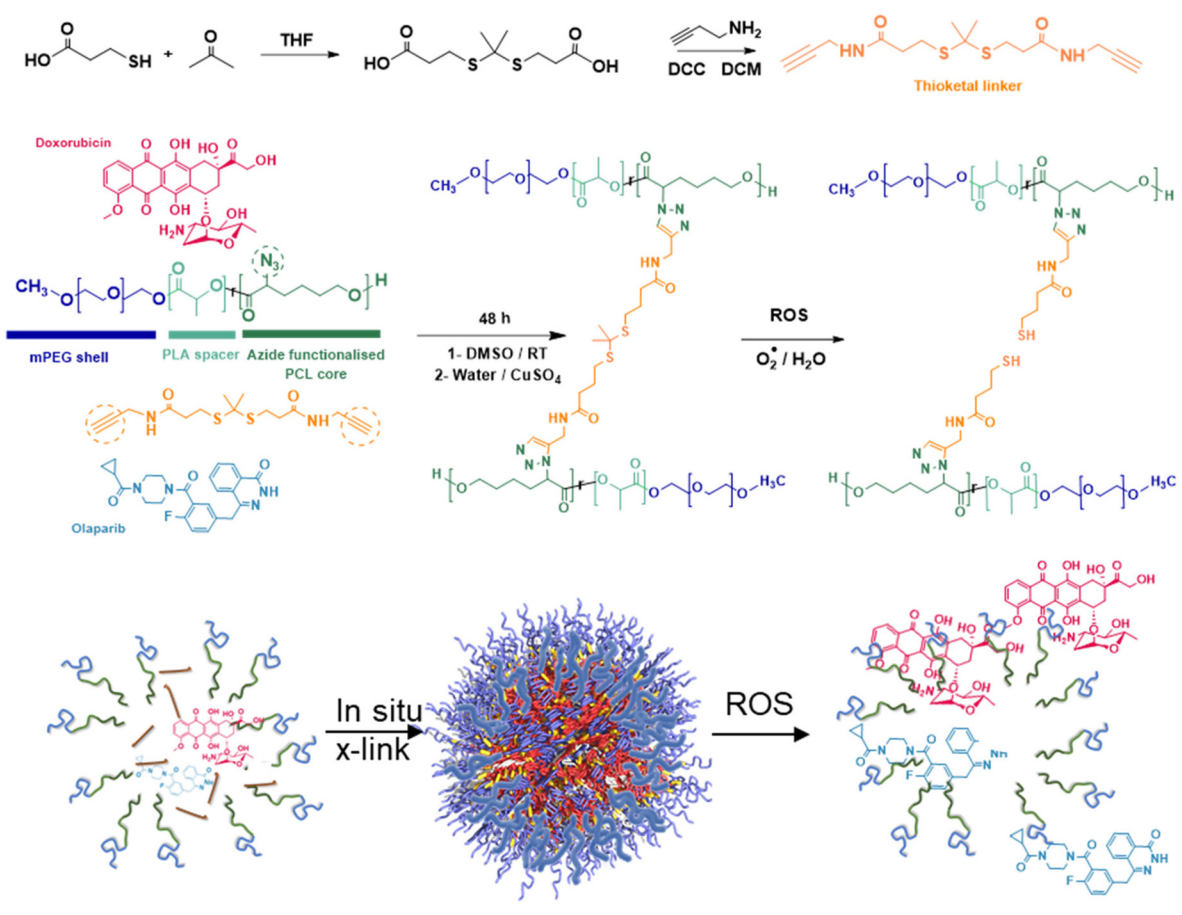

Fig. 6 Synthetic scheme for the preparation of ROS-responsive nanoparticles. A bis(alkynyl) thioketal cross-linker is reacted with mPEG-poly (lactide-*co*-poly(azido-caprolactone)) in the presence of DOX and OLA to form drug-loaded nanoparticles designed to release payload in the presence of reactive oxygen species (ROS).

Open Access Article. Published on 15 Nyenyenyani 2024. Downloaded on 2024-09-11 19:17:30.
This article is licensed under a Creative Commons Attribution 3.0 Unported Licence.

previously. The oxidation-cleavable cross-linker (DTK, Fig. 6) was chosen with a view to potential subsequent application in radiation-treated cells, as first-line interventions for breast cancer usually involve radiotherapy.[30]

In addition, to enable intracellular tracking of the NPs *via* microscopy, Cy5-tagged NPs were prepared *via* reaction of ~1% of the azide groups on the polymeric back bone with alkyne-functional Cy5 fluorophore. 'Core' cross-linking of the polymers was carried out in a similar way, in this case by reacting the azide-groups with 3,3′-(propane-2,2-diylbis(sulfanediyl))bis(*N*-(prop-2-yn-1-yl)propanamide) pre-mixed with/without DOX and OLA in DMSO, with a solution of ascorbic acid followed by copper sulphate in water under a nitrogen atmosphere. Extensive extraction with EDTA solutions was used to remove copper ions which might otherwise be toxic to the cells. The resultant cross-linked polymer nanoparticles were sufficiently colloidally stable that they could be freeze-dried, and when resuspended in water, exhibited diameters of 120–130 nm (Table 2). By varying amounts of drugs in the 'feed' solutions in DMSO, it was possible to encapsulate combinations of DOX : OLA at various ratios. However due to the variability associated with encapsulating two drugs with distinct physiochemical properties, formulating the exact ratios used in initial studies (10 : 1, 1 : 1, 1 : 10) was technically challenging. The exact determined DOX : OLA ratios in the prepared NPs were 13 : 1 (as the closest ratio to 10 : 1), 1 : 1.2 (≈1 : 1) and 1 : 15 (as the closest to the desired 1 : 10). Previous *in vitro* CI synergy assessments (Fig. 1 and 2) demonstrated comparable synergistic effects at 100 : 1 *vs.* 10 : 1 and comparable antagonistic effects at 1 : 10 *vs.* 1 : 100, thus a degree of variation from the exact desired ratios was deemed acceptable. For simplicity these are hereby referred to as their approximate, rounded ratios, however it should be noted that all *in vitro* studies use for control comparison unformulated counterparts at their 'exact' ratio (13 : 1, 1 : 1.2 and 1 : 15).

In the absence of oxidative conditions, the polymer NPs were stable for up to 24 h under the conditions used for cell culture, and did not markedly alter in size or polydispersity when stored at 4 °C (Fig. S4†), but incubation of the polymer NPs with hydrogen peroxide solutions resulted in the rapid loss of discrete particles as evidenced by poor correlation functions in DLS, indicating particle breakdown *via* the oxidising species (Fig. S5†). We chose a hydrogen peroxide solution at much higher concentrations (50 μM) than the reactive oxygen species (ROS) present in normal tissue, but which we reasoned might occur transiently in localised areas of high oxidative stress in cancer cells. Indeed, measurement of ROS levels in breast cancer cell lines using the general oxidative stress indicator probe CM-H2DCFDA indicated raised levels of oxidative species in the cancer cell lines (Fig. S6†). Incubation of cross-linked and non cross-linked polymer NPs, and those prepared with a non-degradable cross-linker,[44] indicated no loss of metabolic activity in MCF-7, MDA-MB-231 and MDA-MB-468 cells, and no evidence of membrane disruption in the absence of encapsulated drugs (Fig. S7†). These experiments suggested that any effects observed in TNBC cells treated with polymer NPs containing drugs would not be due to activities of the carriers, but only the drugs.

Table 2 NP formulation details and characteristics. Drug loadings varied from 3–3.7 weight percent across the formulations

Formulation	Drug combination	Particle size, nm	Polydispersity index
mPEG-*b*-PLA-PCL-DTK 1	—	129	0.05
mPEG-*b*-PLA-PCL-DTK 2	DOX : OLA 13 : 1 (≈10 : 1)	124	0.27
mPEG-*b*-PLA-PCL-DTK 3	DOX : OLA 1 : 1.2 (≈1 : 1)	119	0.06
mPEG-*b*-PLA-PCL-DTK 4	DOX : OLA 1 : 15 (≈1 : 10)	111	0.10

The internalisation of NPs was studied in breast cancer cells (Fig. 7). For these initial studies we prepared non-drug loaded Cy5 labelled NPs (Cy5-NPs) by mixing a labelled mPEG-PLA-PCL polymer, in which a proportion of the azide groups were reacted with Cy5 alkyne, with the mPEG-PLA-PCL-azide prior to cross-linking with the dithioketal. Particle sizing for these NPs was problematic due to absorbance by the Cy5 label close to the laser wavelength of the light scattering instrumentation, but we reasoned that the sizes and charges would be representative of the 'parent' cross-linked polymers as the preparation methods were largely the same.[46] Fluorescence microscopy images demonstrated the uptake and intracellular accumulation of the Cy5-NPs in MCF-7, MDA-MB-231 and MDA-MB-468 cells (Fig. 7A). Image analysis and Cy5-NPs signal quantification revealed that NP internalisation was time-dependent and comparable between cell lines at 0.5 h (Fig. 7B). However, it was found that at 1 h and 2 h, NPs uptake was approximately 2-fold higher in MCF-7 relative to MDA-MB-231 and MDA-MB-468 lines, with the latter two TNBC lines exhibiting similar levels of internalised NPs. Furthermore, the use of Lysotracker dyes enabled the extent of co-localisation of the NPs with active lysosomal compartments to be measured at the 2 h timepoint (Fig. 7C). The Pearson correlation coefficient (PCC) values for NP-Cy5 and Lysotracker labels in MDA-MB-468 and MDA-MB-231 cells at 2 h were 0.58 ± 0.07 and 0.64 ± 0.10, respectively, indicating that a proportion of the NPs were external to lysosomal compartments by this time.

Following confirmation that Cy5-NPs were readily internalised, the uptake of drug combination loaded NPs were studied. Fluorescent cell imaging was used to demonstrate that the drug-loaded NPs (mPEG-*b*-PLA-PCL-DTK 3 formulation; Table 1) were endocytosed and by monitoring the fluorescence of DOX it was possible to show the accumulation of DOX in breast cancer cell nuclei when administered either as free drug or in a polymer NP formulation (Fig. 8).

Image analysis and DOX signal quantification indicated increased DOX delivery *via* NPs to MCF-7 and MDA-MB-468 cell lines relative to free DOX (Fig. 8D). Moreover, the NPs' enhancement of DOX delivery was higher in MCF-7 cells compared to MDA-MB-231 and MDA-MB-468, an observation likely linked to the overall increased Cy5-NPs uptake noted in MCF-7 cells (Fig. 7) and the increased basal ROS levels in this cell line

 This journal is © The Royal Society of Chemistry 2024

Open Access Article. Published on 15 Nyenyenyani 2024. Downloaded on 2024-09-11 19:17:30.
This article is licensed under a Creative Commons Attribution 3.0 Unported Licence.

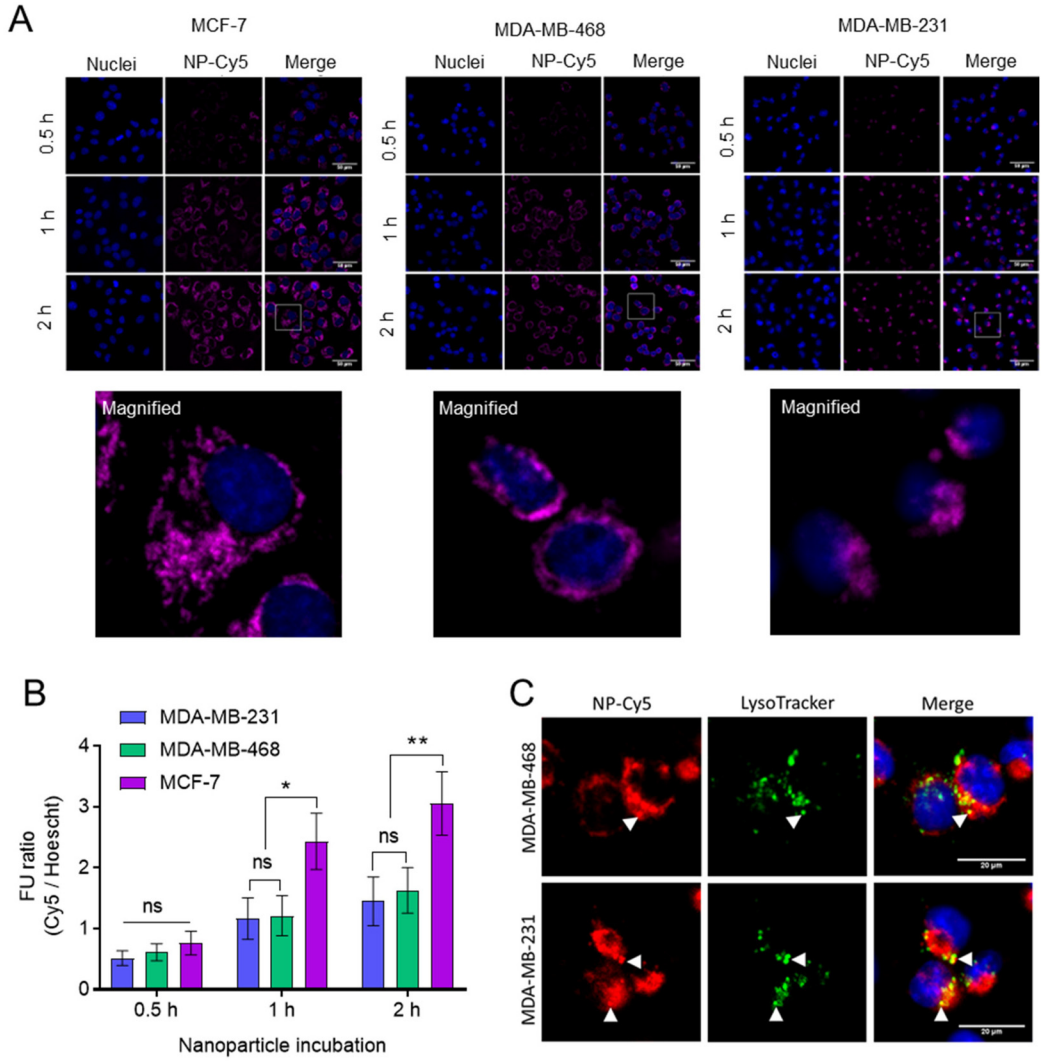

Fig. 7 NP-Cy5 uptake characteristics. (A) NP uptake in BCCs following 0.5, 1 and 2 hours incubation. Scale bar is 50 μm. Magnified sections highlighted with white box are shown underneath. (B) Quantification of NP-Cy5 uptake images. Fluorescent unit (FU) ratio calculated *via* Cy5 signal normalisation to Hoechst nuclear signal. Data presented as mean ± S.D. (C) Lysosomal accumulation of NPs following 2 hours incubation. Staining of lysosomes performed with Lysotracker Green. Scale bar is 20 μm. White triangles indicate co-localisation of NP and lysosome signal. Statistical significance between cell lines tested using one-way ANOVA and Dunnett's multiple comparisons tests (*, $p < 0.05$; **, $p < 0.005$).

relative to TNBC lines which may facilitate increased DOX release from NPs (Fig. S6†). These differences in DOX accumulation may also have been due to the different entry mechanisms for the free drug, *via* organic cation transporters,[47,48] and the polymer carriers which were likely internalised through a range of clathrin-dependent and clathrin-independent pathways.[49]

The effects of DOX : OLA combination NPs were then evaluated in triple negative breast cancer spheroids (Fig. 9 and Table 3). The data demonstrated that increased potency was observed with NPs delivery of the DOX : OLA combinations relative to the unformulated combinations at the corresponding molar ratios. It can be noted that the enhanced potency with NPs was most prominent with combination molar ratios of 10 : 1 (DOX : OLA), with a 2.3 and 2.1-fold increase observed in MDA-MB-468 and MDA-MB-231 cells, respectively (Table 3). NPs containing a DOX : OLA ratio of 1 : 1 induced 1.9 and 1.7-fold increases in potency relative to unformulated combinations in MDA-MB-468 and MDA-MB-231 cells, respectively. No substantial change in potency was noted between NP formulations and unformulated control combinations with the previously determined antagonistic ratio of 1 : 10 in both cell lines tested.

Discussion

Molar ratio-dependent effects

The data gathered here demonstrates that combinations of DOX and OLA can generate synergistic or antagonistic effects

Open Access Article. Published on 15 Nyenyenyani 2024. Downloaded on 2024-09-11 19:17:30.
This article is licensed under a Creative Commons Attribution 3.0 Unported Licence.

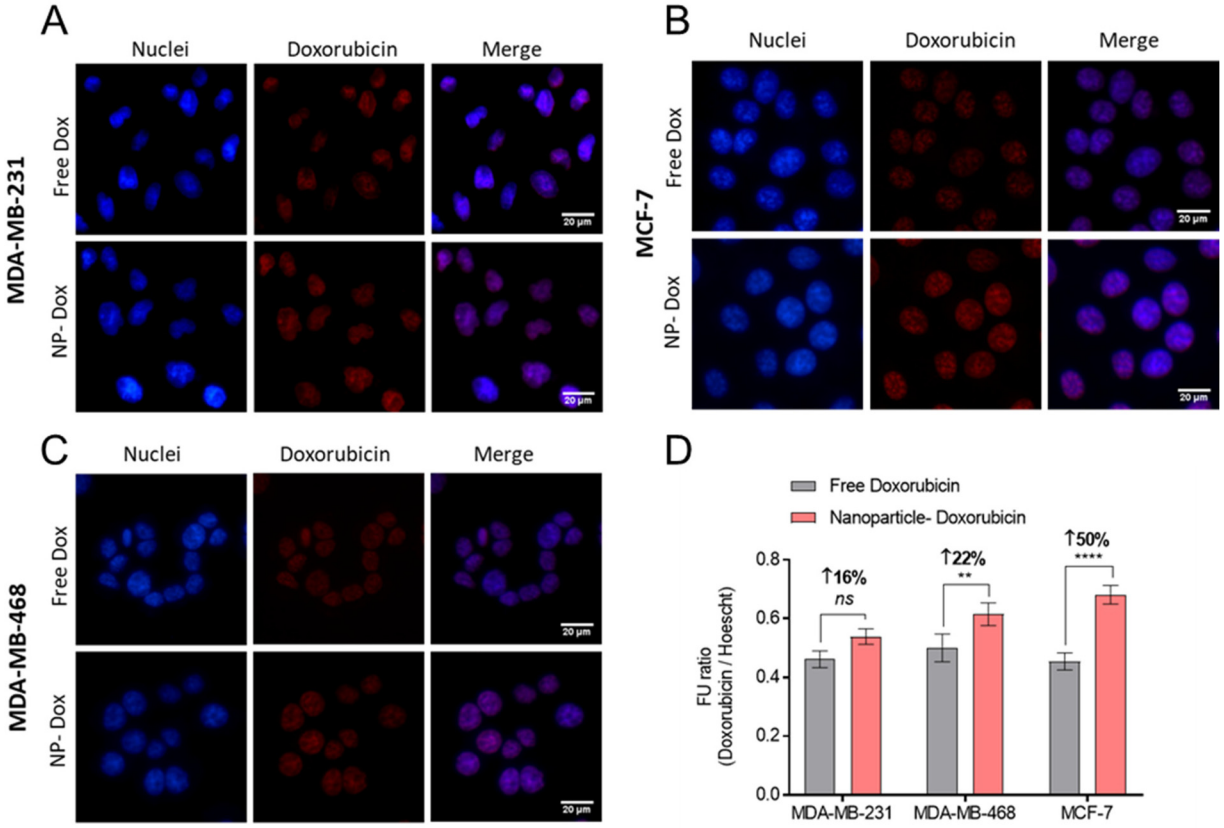

Fig. 8 Doxorubicin delivery in BCCs using NPs. (A–C) Fluorescent micrographs of free doxorubicin and NP-doxorubicin. Doxorubicin treatments applied at 10 μM for 4 hours, followed by counter-staining with DAPI nuclear stain (blue), and PFA-fixation. Scale bars are 20 μM. (D) Quantification of intracellular DOX *via* fluorescence imaging ratioed across doxorubicin and DAPI signals. The NP-Dox formulation studied is mPEG-*b*-PLA-PCL-DTK 3 (Table 1).

in a manner dependent on the molar ratio applied. Thus, for excess DOX (100 : 1, 10 : 1) or equal (1 : 1) ratios, there were synergistic effects in terms of cytotoxic activity, whereas for excess OLA ratios (1 : 10, 1 : 100) there were antagonistic effects. Similar molar ratio dependent activity with these drugs has been observed previously in ovarian cell lines.[50] These observations were consistent across both 2D and 3D *in vitro* models and with the range of assays conducted (Fig. 1 and 2, respectively). In 2D models, metabolic activity testing, used for IC_{50} and CI value calculation, was supported with colony survival studies, the latter testing effects on cell proliferation and colony formation over a series of cell generations. Similarly, in 3D spheroid models, IC_{50} and subsequent CI value determination assessed with ATP measurement (CellTiter Glo assay), correlated with spheroid morphology and size changes following drug treatment. Moreover, varying molar ratios of the drugs in combination were studied, as combination synergy and effects are known to be dependent on molar ratios in addition to distinct drug mechanism of actions.[50,51]

Luminal *vs.* triple negative breast cancer

Single treatment with OLA induced DNA damage and cell killing in both MDA-MB-231 and MCF-7 cells (Table 1 and Fig. 4); interestingly, however, the synergistic effects with DOX, including increased cell death and enhanced DNA damage, were manifest only in triple negative cell lines, and not in the luminal MCF-7 breast cancer cell line (Fig. 4). Further work is required to establish the reasons for this difference; however, it may be hypothesised that the DNA damage response associated with DOX treatments, even though this is not a primary mode of action for DOX, may differ between TNBC and luminal breast cancer, thus resulting in differential sensitisation of DOX by OLA treatment. Moreover, homologous recombination (HR) alterations or deficiencies in TNBC cells[52–54] may further limit available repair mechanisms following DOX insult when combined with PARP inhibition (*via* OLA) and play a role in the synergy observed here. Indeed, several clinical trials are investigating PARP inhibition with OLA to induce synthetic lethality in HR deficient TNBC.[55–58] A potential further explanation of differential DOX/OLA synergy across TNBC and luminal breast cancer cells may be centred around distinct regulation of the transcription repressor Snail, a protein associated with cancer cell survival and EMT. Treatment of MDA-MB-231 cells with DOX in combination with a PARP-inhibitor resulted in an increase in apoptosis compared to cells treated with DOX alone at the same dose.

This journal is © The Royal Society of Chemistry 2024

Open Access Article. Published on 15 Nyenyenyani 2024. Downloaded on 2024-09-11 19:17:30.
This article is licensed under a Creative Commons Attribution 3.0 Unported Licence.

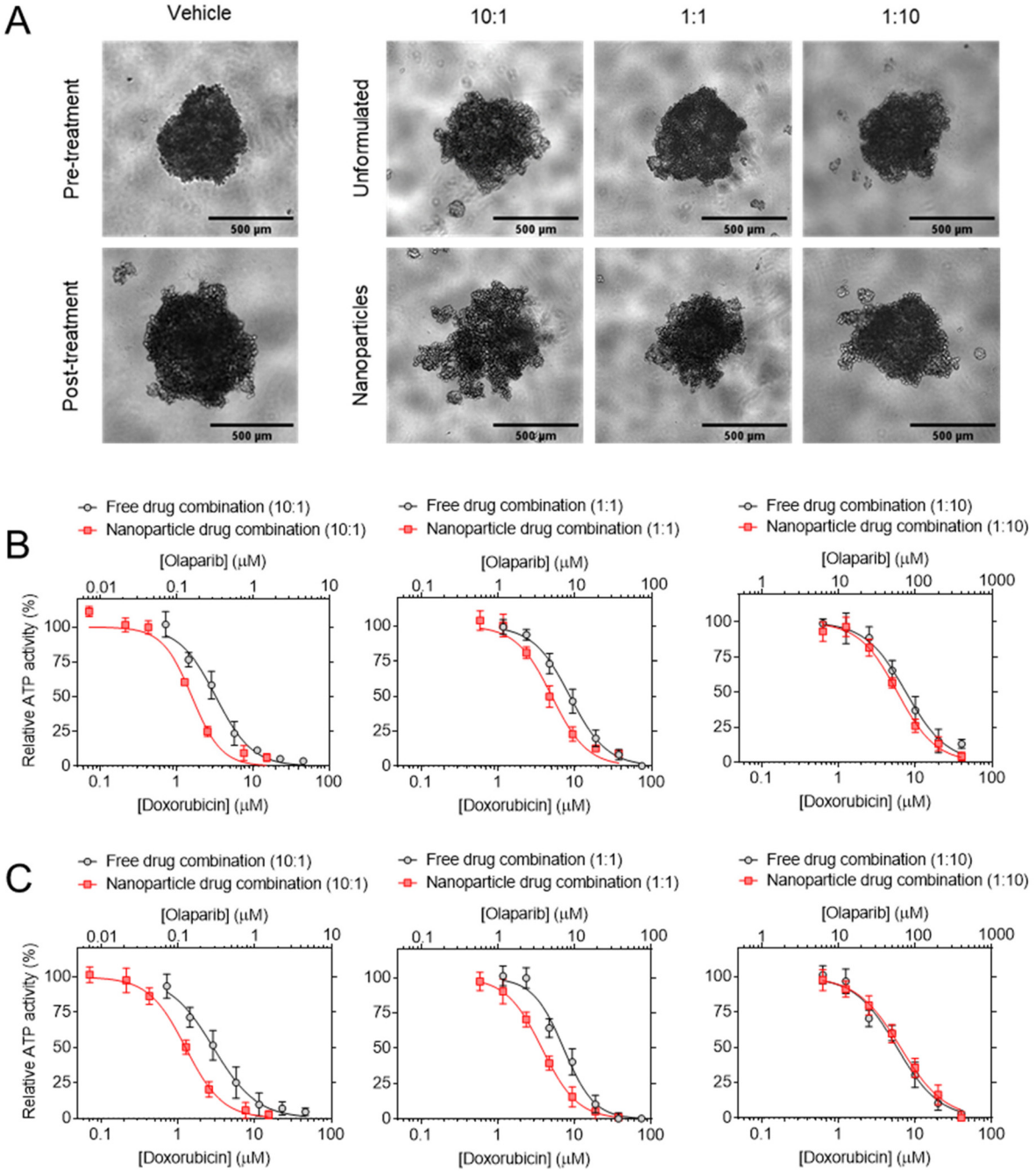

Fig. 9 Cytotoxicity testing of combination NPs. (A) Potency of 10 : 1, 1 : 1 and 1 : 10 DOX : OLA combination NPs in (A) MDA-MB-231 and (B) MDA-MB-468 spheroids. (C) MDA-MB-231 spheroid imaging, scale bar is 500 µm. NPs are compared to their unformulated counterparts based on DOX : OLA molar ratio and calculated IC_{50} values (µM) are displayed in Table 3. Treatments applied for 72 h and assessed for cellular ATP levels using CellTiter Glo 3D assay. Values presented as mean ± S.D and come from three independent experiments.

DOX induced significant increases in Snail expression in several breast cancer cell lines but inhibition of PARP-1 with the investigational compound ABT-888 reduced DOX-induced Snail expression, leading to subsequent increases in apoptotic cell death in these cases.[59] In addition, several reports have demonstrated that cancer cells undergoing epithelial–mesenchymal transition (EMT) exhibit enhanced multidrug resistance.[60–63] In ERα-positive cells, such as MCF-7 cells, resistance to DOX has been reported *via* DOX-induced upregulation of EMT-associated transcription factors, a mechanism shown to be absent in ERα-negative mesenchymal-like cells (MDA-MB-231 and MDA-MB-468).[64] DOX treatment is also reported to induce expression of differing EMT-related proteins (E-cadherin, N-cadherin) in ER positive (MCF-7) and

Open Access Article. Published on 15 Nyenyenyani 2024. Downloaded on 2024-09-11 19:17:30.
This article is licensed under a Creative Commons Attribution 3.0 Unported Licence.

Table 3 Calculated IC_{50} values (μM) of NP combinations and unformulated controls in MDA-MB-231 and MDA-MB-468 3D spheroids. Relevant dose–response graphs shown in Fig. 8. Data presented as mean ± S.E.M. *Nota bene* drug IC_{50} values calculated *via* exact combination ratios (Table 2)

	Control IC_{50} DOX (OLA)	Nanoparticles IC_{50} DOX (OLA)	Fold-increase
MDA-MB-231			
10 : 1	3.28 ± 0.24 (0.25 ± 0.02)	1.59 ± 0.16 (0.12 ± 0.02)	2.1
1 : 1	8.63 ± 0.25 (10.3 ± 0.25)	5.02 ± 0.42 (6.02 ± 0.42)	1.7
1 : 10	7.55 ± 0.14 (113 ± 1.43)	5.84 ± 0.27 (87.6 ± 2.71)	1.3
MDA-MB-468			
10 : 1	2.91 ± 0.15 (0.22 ± 0.02)	1.26 ± 0.12 (0.10 ± 0.01)	2.3
1 : 1	7.20 ± 0.54 (8.64 ± 0.54)	3.76 ± 0.03 (4.51 ± 0.03)	1.9
1 : 10	5.80 ± 0.50 (87.0 ± 5.04)	6.45 ± 0.29 (96.8 ± 2.91)	0.9

negative (MDA-MB-231, MDA-MB-468) cells, while OLA and other PARP inhibitors have been reported to reduce EMT.[65] It is thus possible that the observed synergistic effects seen in our studies with DOX and OLA arose from a combination of enhanced apoptosis and reduced chemoresistance at specific dose ratios. However, antagonistic effects of the drug combinations, observed with cell viability assays (Fig. 1 and 2) were apparent also in MCF-7 cells. This suggests that the OLA-mediated mitochondrial effects noted in triple negative MDA-MB-231 cells (Fig. 5) may also be occurring in MCF-7 cells, although further assays would be required to validate this hypothesis.

Mechanisms of synergistic anti-cancer activity

Induction of DNA double-strand breaks was assessed using immunostaining for the γH2AX foci.[66] In the TNBC line, MDA-MB-231, significantly more γH2AX foci were observed with the synergistic combination ratios of 10 : 1 and 1 : 1 (DOX : OLA) compared to either drug as monotherapy (Fig. 4). At the antagonistic 1 : 10 (DOX : OLA) ratio, significantly decreased γH2AX foci were noted relative to the DOX monotherapy. Furthermore, at this antagonistic ratio foci numbers were not significantly different relative to those induced by OLA at the corresponding combination concentration (10 μM). Together, these observations suggest that the DNA damaging effects of DOX can be enhanced *via* OLA-mediated inhibition of PARP associated DNA repair and subsequently increase apoptosis and cell death. DOX is known to intercalate with DNA and inhibit topoisomerase II, in turn preventing DNA unwinding during transcription to halt DNA replication.[67] In addition to topoisomerase II poisoning *via* trapping topoisomerase II at cleavage sites, DOX has been suggested to induce anticancer activity through inducing DNA strand breakage, either directly through DNA torsion resulting from intercalation[68] or indirectly *via* the generation of ROS and subsequent oxidative stress.[69] We have observed these mechanisms of DNA damage and generation of ROS in the current study (Fig. 4 and 5, respectively) and surmise that they may be responsible for the demonstrated synergy with the PARP1 inhibitor OLA. PARP1 is involved in various DNA damage responses[70] and during the DNA repair process OLA inhibits PARP activity through trapping the enzyme at damaged DNA sites, subsequently preventing repair and additionally inducing DNA lesions through collision and collapse of replication forks.[71]

The use of high OLA concentrations appears however to abrogate DOX-induced DNA damage and this phenomenon may be driven in some part *via* mitochondrial-associated processes whereby DOX-induced ROS is reduced and mitochondrial membrane potential protected (Fig. 5). The current work investigated simultaneous application of drugs, reflecting how co-encapsulated drugs would be delivery *via* nanoparticles, however it is hypothesised synergy may be improved with a regime involving OLA pre-treatment prior to DOX in order to achieve pre-sensitisation.[72]

Nanoparticle uptake and potency

The increased potency of the NPs relative to unformulated combinations may be a result of increased drug delivery, as observed in Fig. 8. This observation of increased drug uptake was based on quantification of DOX, owing to its inherent fluorescence, and the enhanced delivery of this drug alone may have been responsible for the increased potency observed. DOX is a small molecule and can be rapidly transported into cells and enter its target site of action (nuclei) by organic cation transporters and also passive diffusion. Dox-loaded NPs rely however on endocytosis for cell internalisation and subsequence drug release prior to entry into the nuclei. Uptake of DOX into the cell nuclei is critical due to the mechanism of action for this molecule which involves intercalation with DNA to induce cell death. Previous reports indicate that this can be hindered by incomplete DOX release from particles, and this is typically associated with DOX-conjugates[49,73] and nonresponsive NPs with high stability in the cellular environment.[73–76] On the other hand, responsive polymeric materials for NP delivery of DOX have been shown to generate increased nuclear DOX delivery.[75,76] Our studies using Cy5-NPs demonstrate rapid NP cellular uptake within 1 h and presence of the cytoplasmic Cy5-NP signal (Fig. 7). Moreover, this is coupled with DOX-NPs at 2 h showing increased DOX delivery relative to the free drug and a nuclear DOX localisation (Fig. 8). Thus, in the current work the use of oxidative-responsive materials to aid drug release alongside the rapidly internalised NPs are together likely responsible for the increased DOX delivery observed.

A number of studies have demonstrated that the use of carriers for anti-cancer drugs can improve efficacy *in vitro* and/or therapeutic window *in vivo* compared to the free drugs, attributable to different internalisation mechanisms *in vitro* and also altered pharmacokinetic parameters *in vivo*.[77–80] Although the full details of the endocytic mechanisms for the NPs in this study are not yet known, polymers of similar composition and size were internalised by both clathrin-and caveolin-mediated pathways in a range of breast cancer cells,[49] and thus it is likely that these polymers entered by similar routes.

 This journal is © The Royal Society of Chemistry 2024

Open Access Article. Published on 15 Nyenyenyani 2024. Downloaded on 2024-09-11 19:17:30.
This article is licensed under a Creative Commons Attribution 3.0 Unported Licence.

However, it can be hypothesised that OLA delivery is also enhanced with NP formulation, as OLA is subjected to similar drug resistance efflux pumps as DOX, which may be overcome *via* NP-mediated endocytosis.[81] Interestingly, NP formulation of a 1 : 10 DOX : OLA combination resulted in a non-significant effect on potency. The reasons for this are unclear but may be related to the antagonistic effects (mitochondrial protection; Fig. 5) of high OLA concentrations. The theorised increased OLA delivery, and thus increased OLA intracellular accumulation with NP formulation, may be subsequently enhancing mitochondrial-mediated cell survival and protection from DOX cytotoxicity.

It is further possible that the more "DOX-rich" nanoparticles operated *via* a self-catalytic mechanism, in which any initial release of DOX caused the production of ROS species which in turn helped to cleave the oxidation-sensitive cross-links in the NPs, thus releasing more DOX. Confirming such a hypothesis would require *in situ* sensing of ROS generation, which is beyond the scope of this initial investigation, but the observation of enhanced combination potency of synergistic ratios (10 : 1 and 1 : 1) of these drugs in a responsive NP formulation suggests a potential advantage for these systems in future clinical practice. The differing pharmacokinetics of DOX and OLA when administered as free drugs mean that simultaneous delivery to target cells may be difficult to achieve, and thus tumours will be exposed to a range of drug : drug ratios, some of which will be antagonistic. In principle, maintenance of synergistic combination ratios is inherently simpler when the drugs are incorporated within the oxidation-responsive nanoparticles, as release will occur only on cleavage of the thioketal link. In practice, it may be that esterase activity *in vivo* also degrades the NPs to accelerate drug release, but such processes should be slower than those of cross-linker cleavage mediated NP breakdown, thus the systemic release of drug from these NPs is still less likely than the intended intracellular release.

Conclusions

In summary, we have shown that specific ratios of a topoisomerase II inhibitor and a DNA-damage repair inhibitor can exhibit potent and synergistic cytotoxicity in triple negative breast cancer cells in both 2D and 3D cultures. We suggest that the overall effects of the drugs are not simply additive and may arise from a range of different mechanisms, including a potential role of DOX in DNA damage in addition to its well-established topoisomerase II activity. In combination with OLA this resulted in an increase in DNA strand breakage, apoptosis, and cell death in TNBC cell lines. Furthermore, delivery *via* a polymeric carrier with an oxidation-sensitive cross-linker resulted in a further increase in cytotoxicity in 3D spheroids at specific drug : drug ratios, which we suggest is a function of the different entry mechanisms for small molecule drugs compared to nanoparticles. These experiments thus establish a further rationale for drug : drug combinations in breast cancer therapies, the use of nanoparticle formulations to enable controlled delivery of specific synergistic drug ratios and the potential advantages of responsive nanoparticle carriers for co-delivery of these agents.

Materials and methods

Materials

Standard reagents, solvents monomers and other materials for chemical synthesis were purchased from Sigma-Aldrich or ThermoFisher. High glucose DMEM (phenol red free, cat. # 31053-028) was acquired from Gibco (Life technologies). High glucose DMEM (cat. # D6546), Trypsin–EDTA (cat. # T3924), foetal bovine serum (FBS, cat. # F7524), penicillin–streptomycin antibiotic solution (10 000 U penicillin and 10 mg mL^{-1} streptomycin, cat. # P0781), L-glutamine (200 mm, cat. # G7513) and DMSO (cat. # D2438) were purchased from Sigma-Aldrich. Hoechst 33342 (cat. # H1399) and Presto Blue 10× solution (cat. # A13262 100 mL) were acquired from Invitrogen. Cy5 alkyne was purchased from Sigma-Aldrich.

Monomer, cross-linker and polymer synthesis

Synthesis of α-chloro-ε-caprolactone. The chlorocaprolactone monomer was made by a previously reported route,[44] and characterisation data were consistent with those in prior literature for this compound.[82]

Synthesis of 3,3′-(propane-2,2-diylbis(sulfanediyl))dipropionic acid. 3-Mercaptopropionic acid (8.52 g, 6.99 mL, 80.3 mmol) and a catalytic amount of trifluoroacetic acid (TFA, 34 μL) were dissolved in acetone (3 mL, 41 mmol). The mixture was stirred at room temperature for 8 h. Then the resultant white precipitate was filtered and washed with hexane and cold water. The white product was obtained with a yield of 90%.

^{1}H NMR (300 MHz, $CDCl_3$): δ 2.91 (m, 2H), 2.68 (m, 2H), 1.60 (s, 6H).

Synthesis of 3,3′-(propane-2,2-diylbis(sulfanediyl))bis(*N*-(prop-2-yn-1-yl)propanamide). The dithioketal product 3,3′-(propane-2,2-diylbis(sulfanediyl))dipropionic acid (1 g, 3.96 mmol) was dissolved in dichloromethane (50 mL) and the solution cooled in an ice-water bath while stirring. Then HoBT (105 mg, 0.79 mmol) dissolved in a minimum amount of DMF was added, followed by propargylamine (0.87 g, 15.8 mmol) and DMAP (0.96 g, 7.92 mmol). A solution of EDC (2.27 g, 11.9 mmol) in dichloromethane was added dropwise to the reaction mixture at 0 °C, after which the reaction was allowed to warm up to room temperature and stirring was continued overnight. The reaction mixture was washed thoroughly with 0.5 M HCl, aqueous saturated $NaHCO_3$, and brine, then dried over Na_2SO_4 and the solution concentrated by rotary evaporation. The desired product was recovered following silica-gel flash-chromatography using hexanes and acetone as the eluent.

Open Access Article. Published on 15 Nyenyenyani 2024. Downloaded on 2024-09-11 19:17:30.
This article is licensed under a Creative Commons Attribution 3.0 Unported Licence.

Polymer synthesis

Synthesis of mPEG-*b*-poly(D,L-lactide-*co*-αClεCL) diblock polymer. This polymer was synthesized by a previously reported route with minor modifications.[44] D,L-Lactide (1.00 g) and chloro-ε-caprolactone (1.03 g) were transferred into a flask containing mPEG5000 (5.00 g) which was previously dried by azeotropic distillation with anhydrous toluene. The contents were heated at 90 °C and solubilized with 10 mL of anhydrous toluene added into the sealed flask under nitrogen atmosphere. At this moment, $Sn(Oct)_2$ (0.002 g) was added and the reaction was left to proceed at 90 °C for 24 h under stirring. Afterwards, the reaction was cooled to room temperature. The product was dissolved in dichloromethane and precipitated in diethyl ether. It was then filtered and dried under reduced pressure until constant weight was achieved. A white powder was obtained in a 75% yield. ^{1}H NMR (400 MHz, $CDCl_3$, δ in ppm): δ 5.20 (d, J = 6.0 Hz, 5H), 4.28 (dd, J = 37.1, 17.4 Hz, 10H), 3.67 (s, 320H), 3.41 (s, 2), 2.07 (d, J = 40.1 Hz, 7H), 1.67–1.41 (m, 35H).

Synthesis of mPEG-*b*-poly(D,L-lactide-*co*-α-N_3-ε-caprolactone). An aliquot of mPEG-*b*-poly(D,L-lactide-*co*-α-Cl-ε-caprolactone) (1.00 g) was transferred into a flask and dissolved in DMSO (3 mL). Subsequently, sodium azide (0.088 g) was carefully added, and the reaction was allowed to proceed for 24 h at room temperature. The product was dissolved in a small amount of dichloromethane and extracted with diethyl ether to remove DMSO before filtering. The reaction product was then dissolved in toluene and centrifuged to remove the insoluble salts followed by the precipitation of the polymer in diethyl ether. The obtained functionalised copolymer was filtered and dried under reduced pressure until constant weight was achieved. A pale-yellow powder was obtained in a yield of 0.80 g, (80%). ^{1}H NMR (400 MHz, $CDCl_3$, δ in ppm): δ 5.37–5.08 (m, 2H), 4.45–4.08 (m, 2H), 3.67 (s, 133H), 3.40 (s, 1H), 1.70 (d, J = 31.0 Hz, 11H), 1.67–1.40 (m, 10H).

Synthesis of Cy5-labelled mPEG-*b*-poly(D,D-lactide-*co*-α-N_3-ε-caprolactone). Briefly, azide-functional copolymer (110 mg, 0.016 mmol) and Cy5-alkyne (10 mg, 0.0179 mmol) were added into a flask and dissolved in DMSO (2 mL). An ascorbic acid solution (265 μL of 25 mg mL^{-1}) was added, and the reaction was purged with nitrogen and left stirring. Afterwards, $CuSO_4$ (520 μL of 10 mg mL^{-1} solution) was added into the flask and the reaction was allowed to stir overnight at room temperature. EDTA was added (19.04 mg, 0.065 mmol per 2 eq. *vs.* Cu) and the polymer was purified by dialysis to remove any unreacted dye. Subsequently, the labelled polymer was frozen and lyophilised. The conjugation efficiency was determined by fluorescence spectroscopy.

Drug-loaded nanoparticles preparation

For a typical preparation, mPEG-*b*-poly(D,D-lactide-*co*-α-N_3ε caprolactone) polymer (100 mg, ~0.0015 mmol), 3,3′-(propane-2,2-diylbis(sulfanediyl))bis(*N*-(prop-2-yn-1-yl)propanamide) (3.8 mg, 0.012 mmol), with doxorubicin and olaparib in the desired molar ratios (10 : 1, 1 : 1, 1 : 10), were dissolved in DMSO (3 mL) and stirred or sonicated until completely dissolved. A solution of ascorbic acid (0.58 mg, 0.0029 mmol) in double-distilled water (10 mL), previously degassed with argon bubbling, was added dropwise *via* a syringe pump to the DMSO with vigorous stirring followed by copper(II) sulphate (0.47 mg, 0.0029 mmol) in 3 mL double-distilled water. The vial was flushed with argon while stirring at 37 °C, and the reaction was stirred overnight at 37 °C. The copper sulphate and non-entrapped drugs were removed *via* dialysis against double-distilled water containing EDTA (in excess relative to the amount of copper added) for 24 h at room temperature. Total drug loadings varied between 3–3.7 wt%, as determined by HPLC methods.

Quantification of drug loading in NPs

Standard curves for doxorubicin and olaparib were prepared using British Pharmacopoeia (BP) Reference Standards for both drugs, and dual standards were made to quantify two drugs together. Stock standards of DOX and OLA were prepared in DMSO at a concentration of 1 mg mL^{-1}, and then working standards of combined DOX and OLA were prepared using a diluent similar to the mobile phase at time of injection (see below). The concentration of each drug in the standards was 50, 25, 10, 7.5, 2.5, 1 and 0.5 μg mL^{-1}; separate working standards of DOX and OLA were prepared at 10 μg mL^{-1} in the diluent (80 : 20, water/ACN, pH 6.8) for comparison. Polymer samples were prepared by resuspending the dried sample (typically 3.5 mg) in 1 mL diluent with sonication and vortexing. The resultant solution was filtered through a 0.25 μm filter tip to remove any remaining polymer. OLA and DOX concentrations were determined on an Agilent Technologies 1200 Series HPLC system using an ACE Excel 5 C18 column (250 × 4.6 mm id) maintained at 25 °C. A gradient mobile phase of 10 mM sodium phosphate buffer (pH = 6.8) and acetonitrile was employed at a flow rate of 1 mL min^{-1}. 80% aqueous buffer was applied for 5 minutes, linearly decreased to 40% over 15 minutes, before returning to initial conditions over 2 minutes and holding for a further 8 minutes. For OLA, the eluent was monitored using a variable wavelength detector at 254 nm with a peak eluting at a retention time of 15.0 minutes, while for DOX detection, a fluorescence detector at 485/590 nm (ex/em) and a peak eluted at a retention time of 14.1 minutes.

Cell culture

All cells were purchased from the American Type Culture Collection (ATCC; Manassas, Virginia). MDA-MB-231, MCF7 and MDA-MB-468 cells were used in a passage window of 15 and cultured in DMEM (Sigma-Aldrich) supplemented with 10% (v/v) foetal bovine serum (FBS; Sigma-Aldrich) and 2 mM L-glutamine. Culture conditions were maintained at 37 °C with 5% CO_2 and 90% relative humidity.

Cytotoxicity experiments

Drug and nanoparticle potency in 2D cultured cells was evaluated with the PrestoBlue cell viability assay (Thermo Fisher

 This journal is © The Royal Society of Chemistry 2024

Open Access Article. Published on 15 Nyenyenyani 2024. Downloaded on 2024-09-11 19:17:30.
This article is licensed under a Creative Commons Attribution 3.0 Unported Licence.

Scientific). All cell types were seeded at a density of 1×10^4 cells per well in a 96 well plate and cultured for 24 hours prior to assaying. Doxorubicin and Olaparib were exposed to cells for 48 hours applied in 100 μL phenol red free DMEM containing 10% (v/v) FBS. Triton X-100, applied at 1% (v/v) in phenol red free DMEM, was used as a cell death (positive) control and a vehicle control containing no drug used as a negative control. Following exposure, cells were washed twice with PBS and 100 μL 10% (v/v) PrestoBlue reagent diluted in phenol red free medium applied per well for 60 min at 37 °C. The resulting fluorescence was measured at 560/600 nm ($\lambda_{ex}/\lambda_{em}$). Relative metabolic activity was calculated by setting values from the negative control as 100% and positive control values as 0% metabolic activity.

3D spheroid assays

Corning 7007 ultra-low attachment (ULA) 96-well round bottom plates were used to culture the 3D spheroids. MDA-MB-231 and MDA-MB-468 cells were seeded at 2000 cells per well in the presence of Cultrex basement membrane extract (Cultrex-BME, 100 μg mL^{-1}), and MCF-7 cells seeded at 5000 cells per well in the absence of extract. The plates were centrifuged at 300 RCF for 5 min and cultured for 3 days until spheroid formation was confirmed by visual inspection. For dosing, drugs and drug loaded nanoparticles were applied in phenol red free DMEM containing 10% (v/v) FBS and incubated with spheroids for 72 hours. Spheroid volume analysis, from images obtained with a Nikon Ti Eclipse inverted microscope, utilized an open source macro for the Fiji distribution of ImageJ written by Ivanov *et al.*[83] Cellular ATP levels were measured as a proxy of spheroid viability, after 72 hours treatment incubation using the CellTiter-Glo 3D assay (Promega). In these experiments, 150 μL of cell culture media was removed per well and 50 μL CellTiter-Glo 3D reagent added to the remaining 50 μL well volume. The contents of the plate were mixed vigorously for 5 minutes, and the plate was incubated for 25 minutes at room temperature. Following this luminescence was measured on a Tecan Spark 10M plate reader using an integration time of 5000 ms.

Calculation of combination index (CI) values

CI values were determined using the widely established Chou and Talalay method.[38,39] To determine each CI value, cytotoxicity studies performed in either 2D or 3D spheroid BCC culture were conducted on (A) DOX applied as a single drug, (B) OLA as a single drug and (C) DOX : OLA combinations at a series of molar ratios. IC_{50} values were subsequently calculated and CI values determined for each combination based on the Chou and Talalay formula, where D_{SD} is the IC_{50} concentration of DOX, D_{SO} is the IC_{50} concentration of OLA, D_{CD} is the IC_{50} concentration of DOX in combination with OLA and D_{CO} is the IC_{50} concentration of OLA in combination with DOX.

$$CI = \frac{D_{CD}}{D_{SD}} + \frac{D_{CO}}{D_{SO}} + \frac{D_{CD}D_{CO}}{D_{SD}D_{SO}}$$

Using this method, CI values indicate synergy (<0.9), additive effect (0.9–0.1) or antagonism (>1.1).[38,39] Graphpad prism (v7.05) was used to generate a heatmap using a three-colour system based on synergy represented by green, additive effects by yellow and antagonism by red.

Clonogenic cell survival assays

MCF-7 and MDA-MB-231 cells were seeded into 12 well plates at a density of 6×10^4 cells per well and cultured for 24 hours prior to treatment. Cells were exposed for 24 hours to doxorubicin (0.6–60 nM), olaparib (0.3–10 μM) or doxorubicin/olaparib combinations. Treatments were applied in DMEM containing 10% FBS, and this solution alone served as the vehicle control in all experiments. Cells were then harvested using trypsin, counted, and re-seeded at low density for colony formation in drug-free medium in 6 well plates. After 14 days colonies were fixed with 4% formalin solution in PBS, stained with 0.5% crystal violet and counted as a survivor if containing 50 or more cells. All experiments were performed at least thrice. Surviving fraction (SF) was calculated as: number of colonies/(number of cells plated × plating efficiency), where plating efficiency (PE) was defined as: number of control colonies obtained/number of control cells plated. The damage modification ratio (DMR) was calculated by dividing DOX concentration causing 90%, 50% or 10% cell survival in the absence of OLA treatment by the DOX concentration leading to 90%, 50% or 10% cell survival in the presence of OLA at set molar ratios (1 : 10, 1 : 1 or 10 : 1).

Immunofluorescence microscopy of γH2AX

MCF-7 and MDA-MB-231 cells were seeded on LabTek chamber slides (Thermo Fisher Scientific) with 3×10^4 per chamber well and cultured for 24 hours. Cells were then treated with doxorubicin, olaparib or combinations for 24 hours. Cells were fixed with 4% PFA for 15 minutes at room temperature, permeabilised with 0.1% (v/v) Triton X-100 for 15 minutes at room temperature and then blocked with 1.5% (v/v) bovine serum albumin (BSA) in PBS for 60 minutes at room temperature. Cells were then incubated for 2 hours at room temperature with (1 : 1000) mouse monoclonal anti-gH2AX/ser139, washed thrice with PBS and then incubated with (1 : 500) goat anti-mouse IgG AlexaFluor 488 for 1 hour at room temperature. The camber slides were also stained with 0.5 μg mL^{-1} DAPI to visualise nuclei. Slides were washed twice with PBS and then mounted with coverslips and ProLong™ Gold Antifade Mountant. Microscopy was performed using an EVOS M5000 fluorescent microscope, with subsequent image analysis and counting of foci using ImageJ software (v1.5).

Mitochondrial membrane potential

Alterations in mitochondrial membrane potential were assessed by a JC-1 (Biotium) aggregation assay. MDA-MB-231 cells were seeded in 96 well plates at a density of 1×10^4 cells per well, cultured for 24 hours and then incubated with doxorubicin (1 μM), olaparib (0.1, 1.0 or 10.0 μM), or combinations for 5–60 minutes. Following treatment cells were incubated

Open Access Article. Published on 15 Nyenyenyani 2024. Downloaded on 2024-09-11 19:17:30.
This article is licensed under a Creative Commons Attribution 3.0 Unported Licence.

with 5 μg mL^{-1} JC-1 dye for 15 minutes at 37 °C. Fluorescence was read at 550/600 nm ($\lambda_{ex}/\lambda_{em}$) for detection of JC-1 aggregates, and 485/535 nm ($\lambda_{ex}/\lambda_{em}$) for detection of JC-1 monomers. J-aggregate : monomer ratios were then normalized to values induced by the untreated control (set to a value of 1). For JC-1 imaging, live cell fluorescent microscopy was performed on a Nikon Ti Eclipse inverted microscope.

Intracellular ROS detection

MDA-MB-231 cells were seeded in 96 well plates with 1×10^4 cells per well, cultured for 24 hours, followed by incubation with doxorubicin (1 μM), olaparib (0.1, 1.0 or 10.0 μM), or combinations for 5–60 minutes. Intracellular ROS levels were then assessed using 10 μM CM-H2DCFDA probe (Thermo Fisher Scientific), incubated with cells for 30 minutes at 37 °C and applied in HBSS. Resulting fluorescence was measured at 492/520 nm ($\lambda_{ex}/\lambda_{em}$). Measured values were then normalized to the untreated control (set as a value of 1).

Detection of activated caspase-3/7

The CellEvent ® caspase-3/7 green detection reagent (Thermo Fisher Scientific) was employed to evaluate levels of activated caspase-3 or 7. MDA-MB-231 cells were cultured and treated as described above in 96 well plates. After treatment, 100 μl 2% (v/v) CellEvent probe in PBS was applied per well for 30 minutes at 37 °C. Fluorescent intensity was measured at 502/530 nm ($\lambda_{ex}/\lambda_{em}$) and normalized to the untreated control (set as a value of 1).

Live cell fluorescence microscopy

To assess cellular uptake of Cy5-NP, live cell fluorescence microscopy was used to image MDA-MB-231, MDA-MB-468 and MCF-7 cells. All cells were seeded in CellView™ 35 mm diameter glass-bottom cell culture dishes at a density of 2.5×10^5 cells per dish and cultured for 24 hours. Cy5-NPs (50 μg mL^{-1}) were incubated with cells for 30, 60 and 120 minutes at 37 °C with 5% CO_2. Following exposure, NP solutions were removed, and cells washed three times with ice-cold PBS. Cells were then stained with 10 μg mL^{-1} Hoechst 33342 (Thermo-Fisher) or 10 μg mL^{-1} Hoechst 33342 and 50 nM Lysotracker green DND-26 (Thermo-Fisher) applied in Hank's Balanced Salt Solution (HBSS) for 30 min. Staining solution was removed and cells washed twice with PBS. FluoroBrite DMEM was added to wells and cells were imaged on an inverted Nikon Eclipse TE 300 fluorescent microscope on DAPI, FITC and Cy5 filters. Images were processed using ImageJ software (1.52f).

Conflicts of interest

The authors declare no conflicts of interest. Marianne Ashford and Patricia Monteiro are employees and shareholders of AstraZeneca.

Acknowledgements

This work was supported by the Engineering and Physical Sciences Research Council (EPSRC)-UKRI [grant numbers EP/N006615/1; EP/N03371X/1]. This work was also funded by the Royal Society [Wolfson Research Merit Award WM150086] to CA and The Little Princess Trust in partnership with CCLG. The authors thank the Nanoscale and Microscale Research Centre (nmRC) for providing access to instrumentation, Paul Cooling and Douglas Crackett for expert technical help, and Sian Rankin-Turner and Carol Turrill for excellent administrative support. We also thank the School of Life Sciences imaging facility (SLIM) and their staff, particularly Dr Tim Self, for use of their facilities.

References

1 N. Harbeck, F. Penault-Llorca, J. Cortes, M. Gnant, N. Houssami, P. Poortmans, K. Ruddy, J. Tsang and F. Cardoso, *Nat. Rev. Dis. Primers*, 2019, **5**, 66.
2 G. Bianchini, C. De Angelis, L. Licata and L. Gianni, *Nat. Rev. Clin. Oncol.*, 2022, **19**, 91–113.
3 W. D. Foulkes, I. E. Smith and J. S. Reis-Filho, *N. Engl. J. Med.*, 2010, **363**, 1938–1948.
4 P. Boyle, *Ann. Oncol.*, 2012, **23**(Suppl 6), vi7–v12.
5 G. Stockmans, K. Deraedt, H. Wildiers, P. Moerman and R. Paridaens, *Curr. Opin. Oncol.*, 2008, **20**, 614–620.
6 M. De Laurentiis, D. Cianniello, R. Caputo, B. Stanzione, G. Arpino, S. Cinieri, V. Lorusso and S. De Placido, *Cancer Treat. Rev.*, 2010, **36**(Suppl 3), S80–S86.
7 G. Bianchini, J. M. Balko, I. A. Mayer, M. E. Sanders and L. Gianni, *Nat. Rev. Clin. Oncol.*, 2016, **13**, 674–690.
8 K. R. Bauer, M. Brown, R. D. Cress, C. A. Parise and V. Caggiano, *Cancer*, 2007, **109**, 1721–1728.
9 B. A. Kohler, R. L. Sherman, N. Howlader, A. Jemal, A. B. Ryerson, K. A. Henry, F. P. Boscoe, K. A. Cronin, A. Lake, A. M. Noone, S. J. Henley, C. R. Eheman, R. N. Anderson and L. Penberthy, *J. Natl. Cancer Inst.*, 2015, **107**, djv048.
10 Y. Barenholz, *J. Controlled Release*, 2012, **160**, 117–134.
11 J. K. Sicklick, S. Kato, R. Okamura, M. Schwaederle, M. E. Hahn, C. B. Williams, P. De, A. Krie, D. E. Piccioni, V. A. Miller, J. S. Ross, A. Benson, J. Webster, P. J. Stephens, J. J. Lee, P. T. Fanta, S. M. Lippman, B. Leyland-Jones and R. Kurzrock, *Nat. Med.*, 2019, **25**, 744–750.
12 J. A. Perez-Fidalgo, A. Cortés, E. Guerra, Y. García, M. Iglesias, U. Bohn Sarmiento, E. Calvo García, L. Manso Sánchez, A. Santaballa, A. Oaknin, A. Redondo, M. J. Rubio and A. González-Martín, *ESMO Open*, 2021, **6**, 100212.
13 N. D. Donahue, H. Acar and S. Wilhelm, *Adv. Drug Delivery Rev.*, 2019, **143**, 68–96.
14 E. V. Batrakova, S. Li, A. M. Brynskikh, A. K. Sharma, Y. Li, M. Boska, N. Gong, R. L. Mosley, V. Y. Alakhov, H. E. Gendelman and A. V. Kabanov, *J. Controlled Release*, 2010, **143**, 290–301.

 This journal is © The Royal Society of Chemistry 2024

Open Access Article. Published on 15 Nyenyenyani 2024. Downloaded on 2024-09-11 19:17:30.
This article is licensed under a Creative Commons Attribution 3.0 Unported Licence.

15 F. Greco and M. J. Vicent, *Adv. Drug Delivery Rev.*, 2009, **61**, 1203–1213.
16 M. J. Vicent, F. Greco, R. I. Nicholson, A. Paul, P. C. Griffiths and R. Duncan, *Angew. Chem., Int. Ed.*, 2005, **44**, 4061–4066.
17 S. Ghosh, R. Lalani, V. Patel, D. Bardoliwala, K. Maiti, S. Banerjee, S. Bhowmick and A. Misra, *J. Controlled Release*, 2019, **296**, 114–139.
18 S. Rawal and M. M. Patel, *J. Controlled Release*, 2019, **301**, 76–109.
19 Q. Zhang, G. Xiang, Y. Zhang, K. Yang, W. Fan, J. Lin, F. Zeng and J. Wu, *J. Pharm. Sci.*, 2006, **95**, 2266–2275.
20 K. W. Wang, M. L. Jiang, J. L. Zhou, Y. S. Dong, Y. Liu, Q. Y. Zong, P. Sandbhor, N. D. P. Singh and Y. Y. Yuan, *J. Controlled Release*, 2022, **348**, 1004–1015.
21 D. Zhou, Y. Cong, Y. Qi, S. He, H. Xiong, Y. Wu, Z. Xie, X. Chen, X. Jing and Y. Huang, *Biomater. Sci.*, 2015, **3**, 182–191.
22 A. C. Begg, F. A. Stewart and C. Vens, *Nat. Rev. Cancer*, 2011, **11**, 239–253.
23 H. Lu, D. Samanta, L. Xiang, H. Zhang, H. Hu, I. Chen, J. W. Bullen and G. L. Semenza, *Proc. Natl. Acad. Sci. U. S. A.*, 2015, **112**, E4600–E4609.
24 T. Miran, A. T. J. Vogg, N. Drude, F. M. Mottaghy and A. Morgenroth, *FASEB J.*, 2018, **32**, 2803–2813.
25 A. Beatty, L. S. Fink, T. Singh, A. Strigun, E. Peter, C. M. Ferrer, E. Nicolas, K. Q. Cai, T. P. Moran, M. J. Reginato, U. Rennefahrt and J. R. Peterson, *Mol. Cancer Ther.*, 2018, **17**, 264–275.
26 F. L. Sarmiento-Salinas, A. Delgado-Magallon, J. B. Montes-Alvarado, D. Ramirez-Ramirez, J. C. Flores-Alonso, P. Cortes-Hernandez, J. Reyes-Leyva, I. Herrera-Camacho, M. Anaya-Ruiz, R. Pelayo, L. Millan-Perez-Pena and P. Maycotte, *Front. Oncol.*, 2019, **9**, 480.
27 G. Barrera, *ISRN Oncol.*, 2012, **2012**, 137289.
28 I. I. C. Chio and D. A. Tuveson, *Trends Mol. Med.*, 2017, **23**, 411–429.
29 K. D. Tew and D. M. Townsend, *Curr. Opin. Chem. Biol.*, 2011, **15**, 156–161.
30 Y. Zhang and S. G. Martin, *Clin. Oncol.*, 2014, **26**, 289–300.
31 S. Cajot, D. Schol, F. Danhier, V. Preat, M. C. Gillet De Pauw and C. Jerome, *Macromol. Biosci.*, 2013, **13**, 1661–1670.
32 C. Lin, Z. Zhong, M. C. Lok, X. Jiang, W. E. Hennink, J. Feijen and J. F. J. Engbersen, *J. Controlled Release*, 2006, **116**, 130–137.
33 G. Saito, J. A. Swanson and K.-D. Lee, *Adv. Drug Delivery Rev.*, 2002, **55**, 199–215.
34 C. Lin, Z. Zhong, M. C. Lok, X. Jiang, W. E. Hennink, J. Feijen and J. F. J. Engbersen, *Bioconjugate Chem.*, 2007, **18**, 138–145.
35 C. Sun, Z. Wang, Z. Wang, L. Yue, Q. Cheng, Z. Ye, Q.-W. Zhang and R. Wang, *Biomater. Sci.*, 2021, **9**, 1355–1362.
36 L. Yu, M. Zhang, F.-S. Du and Z.-C. Li, *Polym. Chem.*, 2018, **9**, 3762–3773.
37 C. J. Lovitt, T. B. Shelper and V. M. Avery, *BMC Cancer*, 2018, **18**, 41.
38 T. C. Chou, *Cancer Res.*, 2010, **70**, 440–446.
39 T. C. Chou, *Pharmacol. Rev.*, 2006, **58**, 621–681.
40 E. Christidi and L. R. Brunham, *Cell Death Dis.*, 2021, **12**, 339.
41 A. M. Cseh, Z. Fabian, R. Quintana-Cabrera, A. Szabo, K. Eros, M. E. Soriano, F. Gallyas, L. Scorrano and B. Sumegi, *Front. Physiol.*, 2019, **10**, 538.
42 D. B. Zorov, M. Juhaszova and S. J. Sollott, *Biochim. Biophys. Acta*, 2006, **1757**, 509–517.
43 R. Riva, S. Schmeits, F. Stoffelbach, C. Jerome, R. Jerome and P. Lecomte, *Chem. Commun.*, 2005, 5334–5336, DOI: **10.1039/B510282K**.
44 P. F. Monteiro, M. Gulfam, C. J. Monteiro, A. Travanut, T. F. Abelha, A. K. Pearce, C. Jerome, A. M. Grabowska, P. A. Clarke, H. M. Collins, D. M. Heery, P. Gershkovich and C. Alexander, *J. Controlled Release*, 2020, **323**, 549–564.
45 N. Zheng, D. Xie, Z. Y. Zhang, J. Kuang, Y. B. Zheng, Q. Wang and Y. Li, *J. Biomater. Appl.*, 2019, **34**, 326–338.
46 F. Sodano, R. J. Cavanagh, A. K. Pearce, L. Lazzarato, B. Rolando, A. Fraix, T. F. Abelha, C. E. Vasey, C. Alexander, V. Taresco and S. Sortino, *Biomater. Sci.*, 2020, **8**, 1329–1344.
47 H. H. Lee, B. F. Leake, R. B. Kim and R. H. Ho, *Mol. Pharmacol.*, 2017, **91**, 14–24.
48 M. Okabe, M. Unno, H. Harigae, M. Kaku, Y. Okitsu, T. Sasaki, T. Mizoi, K. Shiiba, H. Takanaga, T. Terasaki, S. Matsuno, I. Sasaki, S. Ito and T. Abe, *Biochem. Biophys. Res. Commun.*, 2005, **333**, 754–762.
49 V. Taresco, T. F. Abelha, R. J. Cavanagh, C. E. Vasey, A. B. Anane-Adjei, A. K. Pearce, P. F. Monteiro, K. A. Spriggs, P. Clarke, A. Ritchie, S. Martin, R. Rahman, A. M. Grabowska, M. B. Ashford and C. Alexander, *Adv. Ther.*, 2020, **4**, 2000103.
50 S. Eetezadi, J. C. Evans, Y. T. Shen, R. De Souza, M. Piquette-Miller and C. Allen, *Mol. Pharm.*, 2018, **15**, 472–485.
51 A. Dicko, L. D. Mayer and P. G. Tardi, *Expert Opin. Drug Delivery*, 2010, **7**, 1329–1341.
52 J. Staaf, D. Glodzik, A. Bosch, J. Vallon-Christersson, C. Reuterswärd, J. Häkkinen, A. Degasperi, T. D. Amarante, L. H. Saal, C. Hegardt, H. Stobart, A. Ehinger, C. Larsson, L. Rydén, N. Loman, M. Malmberg, A. Kvist, H. Ehrencrona, H. R. Davies, Å. Borg and S. Nik-Zainal, *Nat. Med.*, 2019, **25**, 1526.
53 N. C. Turner, *N. Engl. J. Med.*, 2017, **377**, 2490–2492.
54 P. Polak, J. Kim, L. Z. Braunstein, R. Karlic, N. J. Haradhavala, G. Tiao, D. Rosebrock, D. Livitz, K. Kübler, K. W. Mouw, A. Kamburov, Y. E. Maruvka, I. Leshchiner, E. S. Lander, T. R. Golub, A. Zick, A. Orthwein, M. S. Lawrence, R. N. Batra, C. Caldas, D. A. Haber, P. W. Laird, H. Shen, L. W. Ellisen, A. D. D'Andrea, S. J. Chanock, W. D. Foulkes and G. Getz, *Nat. Genet.*, 2017, **49**, 1476–1486.

Open Access Article. Published on 15 Nyenyenyani 2024. Downloaded on 2024-09-11 19:17:30.
This article is licensed under a Creative Commons Attribution 3.0 Unported Licence.

55 B. Kaufman, R. Shapira-Frommer, R. K. Schmutzler, M. W. Audeh, M. Friedlander, J. Balmaña, G. Mitchell, G. Fried, S. M. Stemmer, A. Hubert, O. Rosengarten, M. Steiner, N. Loman, K. Bowen, A. Fielding and S. M. Domchek, *J. Clin. Oncol.*, 2015, **33**, 244–250.
56 M. Robson, S. A. Im, E. Senkus, B. H. Xu, S. M. Domchek, N. Masuda, S. Delaloge, W. Li, N. Tung, A. Armstrong, W. T. Wu, C. Goessl, S. Runswick and P. Conte, *N. Engl. J. Med.*, 2017, **377**, 523–533.
57 M. E. Robson, S. A. Im, E. Senkus, B. H. Xu, S. M. Domchek, N. Masuda, S. Delaloge, N. D. E. Tung, A. Armstrong, M. Dymond, A. Fielding, A. Allen and P. Conte, *Eur. J. Cancer*, 2023, **184**, 39–47.
58 J. J. J. Geenen, S. C. Linn, J. H. Beijnen and J. H. M. Schellens, *Clin. Pharmacokinet.*, 2018, **57**, 427–437.
59 G. Mariano, M. R. Ricciardi, D. Trisciuoglio, M. Zampieri, F. Ciccarone, T. Guastafierro, R. Calabrese, E. Valentini, A. Tafuri, D. Del Bufalo, P. Caiafa and A. Reale, *Oncotarget*, 2015, **6**, 15008–15021.
60 K. R. Fischer, A. Durrans, S. Lee, J. Sheng, F. Li, S. T. Wong, H. Choi, T. El Rayes, S. Ryu, J. Troeger, R. F. Schwabe, L. T. Vahdat, N. K. Altorki, V. Mittal and D. Gao, *Nature*, 2015, **527**, 472–476.
61 X. Zheng, J. L. Carstens, J. Kim, M. Scheible, J. Kaye, H. Sugimoto, C. C. Wu, V. S. LeBleu and R. Kalluri, *Nature*, 2015, **527**, 525–530.
62 T. Xu, J. Zhang, W. Chen, S. Pan, X. Zhi, L. Wen, Y. Zhou, B. W. Chen, J. Qiu, Y. Zhang, Q. Yang, X. Feng, X. Bai and T. Liang, *Cancer Lett.*, 2016, **377**, 140–148.
63 M. El Amrani, F. Corfiotti, M. Corvaisier, R. Vasseur, M. Fulbert, C. Skrzypczyk, A. C. Deshorgues, V. Gnemmi, D. Tulasne, F. Lahdaoui, A. Vincent, F. R. Pruvot, I. Van Seuningen, G. Huet and S. Truant, *Mol. Carcinog.*, 2019, **58**, 1985–1997.
64 X. Wan, J. Hou, S. Liu, Y. Zhang, W. Li, Y. Zhang and Y. Ding, *Front. Cell Dev. Biol.*, 2021, **9**, 583572.
65 M. Schacke, J. Kumar, N. Colwell, K. Hermanson, G. A. Folle, S. Nechaev, A. Dhasarathy and L. Lafon-Hughes, *Int. J. Mol. Sci.*, 2019, **20**, 518.
66 L. J. Kuo and L. X. Yang, *In Vivo*, 2008, **22**, 305–309.
67 D. A. Gewirtz, *Biochem. Pharmacol.*, 1999, **57**, 727–741.
68 F. Yang, S. S. Teves, C. J. Kemp and S. Henikoff, *Biochim. Biophys. Acta*, 2014, **1845**, 84–89.
69 C. F. Thorn, C. Oshiro, S. Marsh, T. Hernandez-Boussard, H. McLeod, T. E. Klein and R. B. Altman, *Pharmacogenet. Genomics*, 2011, **21**, 440–446.
70 A. Ray Chaudhuri and A. Nussenzweig, *Nat. Rev. Mol. Cell Biol.*, 2017, **18**, 610–621.
71 J. Murai, S. Y. Huang, B. B. Das, A. Renaud, Y. Zhang, J. H. Doroshow, J. Ji, S. Takeda and Y. Pommier, *Cancer Res.*, 2012, **72**, 5588–5599.
72 U. A. Matulonis and B. J. Monk, *Ann. Oncol.*, 2017, **28**, 443–447.
73 B. S. Chhikara, D. Mandal and K. Parang, *J. Med. Chem.*, 2012, **55**, 1500–1510.
74 W. L. Ye, J. B. Du, B. L. Zhang, R. Na, Y. F. Song, Q. B. Mei, M. G. Zhao and S. Y. Zhou, *PLoS One*, 2014, **9**, e97358.
75 C. Cui, Y. N. Xue, M. Wu, Y. Zhang, P. Yu, L. Liu, R. X. Zhuo and S. W. Huang, *Biomaterials*, 2013, **34**, 3858–3869.
76 W. Chen, P. Zhong, F. Meng, R. Cheng, C. Deng, J. Feijen and Z. Zhong, *J. Controlled Release*, 2013, **169**, 171–179.
77 M. Gulfam, T. Matini, P. F. Monteiro, R. Riva, H. Collins, K. Spriggs, S. M. Howdle, C. Jerome and C. Alexander, *Biomater. Sci.*, 2017, **5**, 532–550.
78 C. J. Bowerman, J. D. Byrne, K. S. Chu, A. N. Schorzman, A. W. Keeler, C. A. Sherwood, J. L. Perry, J. C. Luft, D. B. Darr, A. M. Deal, M. E. Napier, W. C. Zamboni, N. E. Sharpless, C. M. Perou and J. M. DeSimone, *Nano Lett.*, 2017, **17**, 242–248.
79 G. Sahay, E. V. Batrakova and A. V. Kabanov, *Bioconjugate Chem.*, 2008, **19**, 2023–2029.
80 T. Minko, E. V. Batrakova, S. Li, Y. L. Li, R. I. Pakunlu, V. Y. Alakhov and A. V. Kabanov, *J. Controlled Release*, 2005, **105**, 269–278.
81 H. L. Wong, R. Bendayan, A. M. Rauth, H. Y. Xue, K. Babakhanian and X. Y. Wu, *J. Pharmacol. Exp. Ther.*, 2006, **317**, 1372–1381.
82 S. Lenoir, R. Riva, X. Lou, C. Detrembleur, R. Jérôme and P. Lecomte, *Macromolecules*, 2004, **37**, 4055–4061.
83 D. P. Ivanov, A. M. Grabowska and M. C. Garnett, *Methods Mol. Biol.*, 2017, **1601**, 43–59.

This journal is © The Royal Society of Chemistry 2024